GEOSPHERE

GEOSPHERE, v. 18, no. 6

https://doi.org/10.1130/GES02526.1

18 figures; 2 tables

CORRESPONDENCE: gav4@buffalo.edu

CITATION: Valentine, G.A., Fierstein, J., and White J.D.L., 2022, Pyroclastic deposits of Ubehebe Crater Death Valley, California, USA: Ballistics, pyroclastic surges, and dry granular flows: Geosphere, v. 18, no. 6, p. 1926-1957, https://doi.org/10.1130/GES02526.1.

Science Editor: Christopher J. Spencer Associate Editor: Nick Lang

Received 24 February 2022 Revision received 10 June 2022 Accepted 24 August 2022

Published online 4 November 2022





This paper is published under the terms of the CC-BY-NC license

© 2022 The Authors

Pyroclastic deposits of Ubehebe Crater, Death Valley, California, **USA: Ballistics, pyroclastic surges, and dry granular flows**

Greg A. Valentine¹, Judy Fierstein², and James D.L. White³

Department of Geology, 126 Cooke Hall, University at Buffalo, Buffalo, New York 14260, USA ²U.S. Geological Survey, Volcano Science Center, 345 Middlefield Road, Menlo Park, California 94025, USA ³Department of Geology, University of Otago, P.O. Box 56, Dunedin 9054, New Zealand

ABSTRACT

We describe and interpret deposits associated with the final Ubehebe Crater-forming, phreatomagmatic explosive phase of the multivent, monogenetic Ubehebe volcanic center. Ubehebe volcano is located in Death Valley, California, USA. Pyroclastic deposits occur in four main facies: (1) lapilli- and block-dominated beds, (2) thinly bedded lapilli tuff, (3) laminated and cross-laminated ash, and (4) massive lapilli ash/tuff. Lapilli- and block-dominated beds are found mostly within several hundred meters of the crater and transition outward into discontinuous lenses of lapilli and blocks; they are interpreted to have been deposited by ballistic processes associated with crater-forming explosions. Thinly bedded lapilli tuff is found mainly within several hundred meters, and laminated and cross-laminated ash extends at least 9 km from the crater center. Dune forms are common within ~2 km of the crater center, while finer-grained, distal deposits tend to exhibit planar lamination. These two facies (thinly bedded lapilli tuff and laminated and cross-laminated ash) are interpreted to record multiple pyroclastic surges (dilute pyroclastic currents). Repeated couplets of coarse layers overlain by finer-grained, laminated horizons suggest that many or most of the surges were transient, likely recording individual explosions, and they traveled over complex topography in some areas. These two factors complicate the application of classical sediment-transport theory to quantify surge properties. However, duneform data provide possible constraints on the

Greg Valentine https://orcid.org/0000-0002-8133-5878

relationships between suspended load sedimentation and bed-load transport that are consistent using two independent approaches. Massive lapilli ash/tuff beds occur in drainages below steep slopes and can extend up to ~1 km onto adjacent valley floors beneath large catchments. Although they are massive in texture, their grainsize characteristics are shared with laminated and cross-laminated ash facies, with which they are locally interbedded. These are interpreted to record concentrated granular flows sourced by remobilized pyroclastic surge deposits, either during surge transport or shortly after, while the surge deposits retained their elevated initial pore-gas pressures. Although similar surge-derived concentrated flows have been described elsewhere (e.g., Mount St. Helens, Washington, USA, and Soufriére Hills, Montserrat, West Indies), to our knowledge Ubehebe is the first case where such processes have been identified at a maar volcano. These concentrated flows followed paths that were independent of the pyroclastic surges and represent a potential hazard at similar maar volcanoes in areas with complex terrain.

■ INTRODUCTION

In the 1960s, researchers studying the deposits around maars-volcanic craters that cut into the pre-eruptive landscape - documented the presence of dune-bedded ash deposits (Moore, 1967; Fisher and Waters, 1970). This work led to the concept of volcanic base surges as ground-hugging, turbulent currents of gas and clasts that flow outward from eruption sites, similar to base surges observed

during buried or submerged nuclear weapons tests (see Fisher et al., 1997). One of the sites of these classic studies was Ubehebe Crater in Death Valley, California, USA (Fisher and Waters, 1970; Crowe and Fisher, 1973).

Our understanding of pyroclastic deposits and the processes that produce them has advanced dramatically in the decades since that seminal research through continued study of deposits, observations of eruptions, experiments, and theoretical/numerical modeling. We now understand that pyroclastic deposits are emplaced by three main mechanisms: (1) pyroclastic currents, which are gas-particle mixtures that flow along the ground because they are denser than the ambient air and produce a variety of deposits (see below); (2) fallout, which leaves well-sorted deposits that mantle the landscape and thin gradually away from source; and (3) ballistic emplacement of coarse lapilli, blocks, and bombs. Pyroclastic currents fall on a spectrum, on one end of which are dilute mixtures (particle concentrations of ~0.1 vol% to a few volume percent; Weit et al., 2018) that transport clasts on the proximal-to-distal scale by turbulent suspension and deposit them through bed-load mechanisms. We refer to these dilute currents as pyroclastic surges, a term that evolved from volcanic base surge; their deposits are typically stratified and cross-stratified, moderately sorted layers that drape the terrain and are thinner at topographic highs than at lows (Fisher and Schmincke, 1984). On the other end of the spectrum are concentrated granular dispersions (~20-50 vol% particles; e.g., Roche, 2015; Valentine, 2020), in which pore-gas pressure and grain-grain interactions affect mobility. These are also called pyroclastic flows, and they produce massive,

poorly sorted deposits that pond in topographic lows. In a sense, pyroclastic surges and flows are the dry, hot volcanic equivalents of sediment transport in typical fluvial flows, with suspended and bed loads, compared to high particle concentration debris flows. Because of this, theoretical research on pyroclastic surge deposition has borrowed heavily from the fluvial sediment-transport literature (Valentine, 1987; Dioguardi and Dellino, 2014; Roche, 2015; Dellino et al., 2019, 2020). Recent largescale experiments are proving especially useful in understanding the links between pyroclastic surge dynamics and their deposits (Dellino et al., 2007, 2020; Brosch and Lube, 2020). Pyroclastic flows have been more elusive in terms of quantifying transport dynamics from deposit characteristics, with recent advances using entrained substrate clasts to estimate flow speeds based upon experimentally derived relations (Roche et al., 2013, 2016). Ballistic emplacement has typically been inferred for individual blocks and bombs or isolated clusters of them (e.g., Gurioli et al., 2013; Breard et al., 2014), but experiments indicate that continuous proximal layers can be emplaced due to discrete explosions of so-called ballistic curtains consisting of outwardand downward-propagating walls of ejected debris (analogous to ejecta curtains in the meteorite impact literature; Graettinger et al., 2014, 2015a). If an explosion occurs within a well-developed crater, ballistic trajectories may be vertically focused to form collimated jets (limited range of ejection angles), or may produce inclined jets where a ballistic curtain propagates to one side of a crater due to pre-explosion topography (e.g., Taddeucci et al., 2013; Valentine et al., 2012, 2015; Graettinger et al., 2015b). Collimated jets may collapse back into the crater, but in experiments some were observed to lean sideways as they collapsed; these can deposit clasts outside of the crater as localized clast showers with limited outward propagation. This process is not to be confused with more traditional mechanisms of fallout from buoyant columns (e.g., Sparks et al., 1997). Some estimates of ejection velocities and angles have been made using the size, shape, and final location of individual ballistic clasts relative to vent (e.g., Self et al., 1980; Valentine et al., 2011), and recently explosion energies and depths

have been estimated from inferred ballistic curtain deposits (Graettinger and Valentine, 2017).

Here, we revisit the exceptionally exposed deposits associated with Ubehebe Crater, which formed during the final and most violent phreatomagmatic phase of the volcanic center's complex eruptive episode, focusing on detailed characterization of the deposits and assessment of the emplacement processes. After an overview of the setting and previous work, we describe the overall stratigraphy and its variations with distance from vent and local topography. The main deposit facies are defined, and we subsequently detail their characteristics and the eruption and emplacement dynamics they record. While previous work emphasized the presence of cross stratification and dune forms, we suggest that ballistic emplacement of coarse beds was also a key contributor in proximal to medial areas. Most of Ubehebe Crater's deposits were emplaced by pyroclastic surges onto a range of topographic settings, from relatively smooth plains to very rugged and steep-sided ridges and gulches. One of the facies records rapid remobilization of fresh pyroclastic surge deposits on these steep slopes, which formed concentrated, dry granular flows that moved independently of their parent surges.

SETTING AND PREVIOUS WORK

Geologic Setting and Eruptive Sequence

Ubehebe volcanic center is located in northern Death Valley, California, and is of trachybasaltic composition (herein loosely referred to as basaltic; Crowe and Fisher, 1973). The center experienced a complex eruptive episode that produced two small cones and 12 explosion craters distributed over ~1.75 km² in two rough alignments (Fig. 1). Fierstein and Hildreth (2017) established the overall stratigraphy and sequence of events for the center, showing that activity commenced with development of a scoria cone that was subsequently destroyed (see below) and associated fallout deposit (S-scoria), and then transitioned to laterally migrating, crater-producing explosion centers. A small second cone (Little Hebe; Fig. 1), dominated by partly welded

spatter, formed within one of the early explosion craters; it was followed by explosions from P Crater, and finally by the formation of Ubehebe Crater sensu stricto (Fig. 1; note that Ubehebe Crater is a part of the overall Ubehebe volcanic center). Ejecta from Ubehebe Crater that rests upon the S-scoria cone deposits are locally thermally altered (Fierstein and Hildreth, 2017), which demonstrates that the entire eruptive sequence occurred within a short enough time span that the initial scoria was still hot when the final Ubehebe Crater-producing explosions occurred; thus, the volcanic center as a whole is monogenetic in that it was produced during a single eruptive episode (Valentine and Connor, 2015). Champion et al. (2018) presented evidence that the eruptive episode took place ~2100 years ago, making Ubehebe one of the youngest intraplate volcanic centers in the southwestern United States (Valentine et al., 2021a).

Ubehebe Crater has a diameter of ~800 m and is 150 m deep. It formed on a ridge of tilted and faulted Miocene fanglomerate that is exposed in the crater walls, in gulches to the east of the crater, and on Tin Mountain to the south-southeast (Fig. 1; Crowe and Fisher, 1973). The fanglomerate is composed of variably indurated arkosic sandstones and conglomerate layers. Pebbles, cobbles, and boulders in the conglomerates include metamorphic, plutonic, and less-abundant Miocene volcanic rocks derived from surrounding mountains. The rounded clasts in the conglomerate locally exhibit throughgoing fractures initiated at clast-clast contact points. Ubehebe Crater's explosions destroyed most of the S-scoria cone, leaving only a remnant that is now exposed in the crater walls and blanketed with ejecta from the Ubehebe Crater, as are Little Hebe and all of the other craters and their deposits. Ubehebe Crater deposits have been found ~9 km to the north and ~7 km to the south of the crater center and likely extended farther in directions unimpeded by high terrain. They can be traced ~4.2 km to the northwest and ~3 km to the east of the crater center. Framework-supported S-scoria fallout underlies Ubehebe Crater deposits at most locations (except for the most distal southern locations). The morphology of the crater and the character of its ejecta deposits are consistent with its formation having been dominated by subsurface

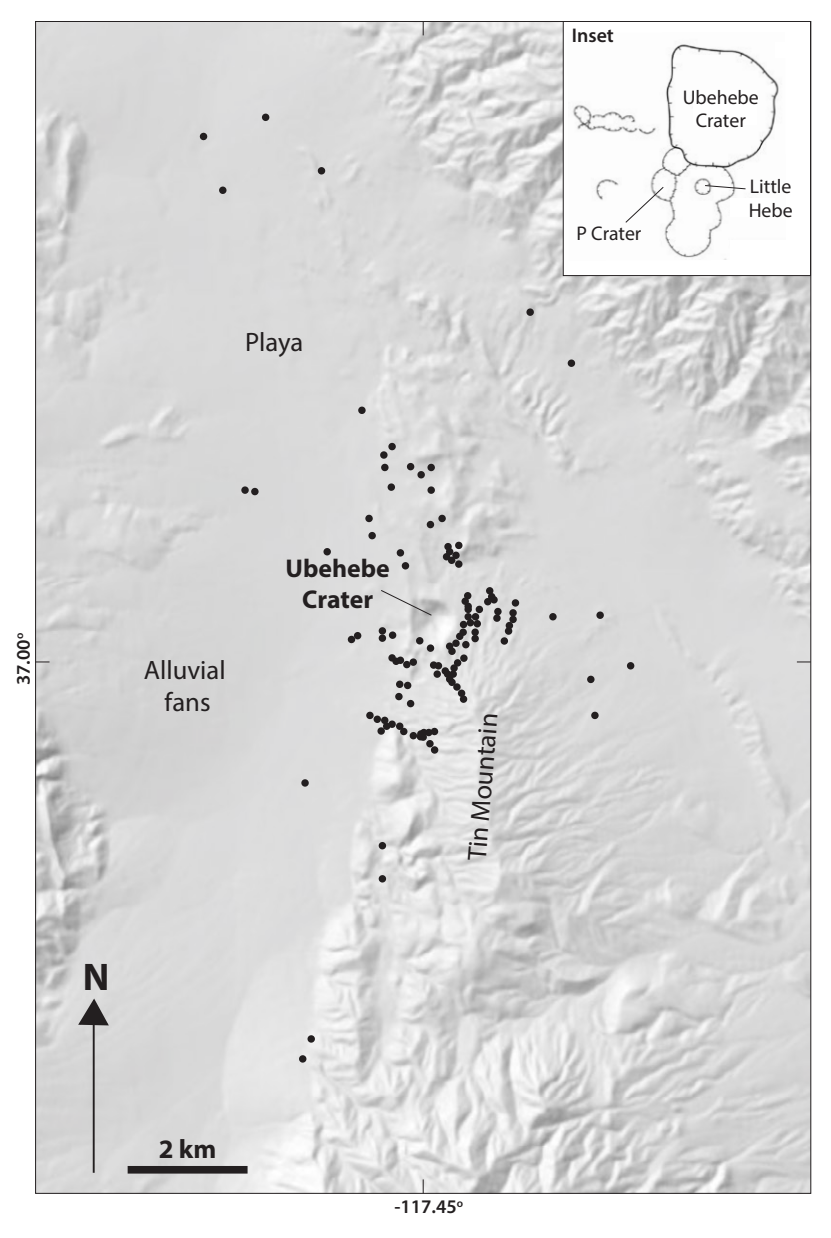


Figure 1. Shaded relief map shows study sites (black dots) with documented Ubehebe Crater deposits (see Table A1 for coordinates and brief descriptions) and major features mentioned in the text (shaded relief from https://apps.nationalmap.gov/3depdem/). Inset shows crater outlines with Little Hebe, P Crater, and Ubehebe Crater labeled.

phreatomagmatic explosions, as has been inferred since the original work of Crowe and Fisher (1973).

Previous Work

Early studies of pyroclastic surge deposits at Ubehebe focused almost entirely on dune forms and cross-stratified deposits because production of such deposits by a volcanic process was a novel finding at the time. Fisher and Waters (1970) provide eloquent descriptions of a few Ubehebe dune forms. Crowe and Fisher (1973) documented more details of the stratified Ubehebe Crater deposits. They showed that the inferred surge deposits are better sorted than most pyroclastic flow deposits, but cross stratification demonstrates emplacement by lateral currents rather than by fallout. Planar beds near the crater rim are coarser grained, but with sorting more consistent with fallout mechanisms, and Crowe and Fisher (1973) argued that they transition laterally to pyroclastic surge deposits, although gaps in exposure prevented us from verifying this. They also considered only three emplacement mechanisms for layers-pyroclastic flow, pyroclastic surge, and fallout-and did not consider ballistic curtain mechanisms, which had not yet been identified. Wohletz and Sheridan (1979) included Ubehebe in their statistical study of pyroclastic surge facies at several maar volcanoes.

Additional work on Ubehebe Crater deposits focused on soft-sediment deformation structures. Douillet et al. (2015) included detailed descriptions of the varieties of such structures, which range from impact sags to flame-like features to contorted beds that have been folded and thrust faulted on scales of decimeters to meters. Valentine et al. (2021b) discussed how there is no independent evidence for the deposits having been emplaced in a damp state; no other indicative features such as accretionary lapilli, depositionally vesiculated tuffs, or mud lumps have been found in our studies. Nor is there any evidence for rainfall events during the eruptive activity (e.g., raindrop impressions or V-shaped gullies within the eruptive sequence; Fierstein and Hildreth, 2017), which might have saturated deposits and facilitated slumping. Valentine et al. (2021b) concluded that the soft-sediment deformation occurred in dry deposits.

Because Douillet et al. (2015) already provide excellent descriptions of the variety of soft-sediment deformation structures, we do not present a general characterization of them but instead discuss the structures within the context of individual facies.

TERMS AND METHODS

Terms

We use standard terms for grain size (e.g., ash, lapilli, block, and bomb) and field-based grain-size distribution (e.g., tuff, lapilli tuff, and tuff breccia; White and Houghton, 2006). The terms stratification and cross stratification are not specific to the thickness of layers in a horizon, but lamination and cross lamination imply individual layer thicknesses of <1 cm. Thin and very thin layers are 3–10 cm and 1–3 cm, respectively (Fisher and Schmincke, 1984).

Previous authors have used different terms for wavy bed forms, such as antidune, dune, and sandwave. Fisher and Waters (1970) used the term antidune based upon low angle dips of strata on lee and stoss sides, but for some readers, antidune may also imply up-current crest migration and/or supercritical flow (see Douillet, 2021). To avoid potential confusion associated with these terms, we use dune form where the shape of the bed form is discernible. Cross stratification of any type was likely originally associated with dune forms, but the forms may not be discernible in outcrop.

Clast types are generally divided into basalt and lithic. Because our focus is on the Ubehebe Craterforming activity, we do not refer to basalt clasts as juvenile unless there is clear evidence that they are primary juvenile in the sense of having potentially contributed heat energy to the explosion that emplaced them (such evidence may include fluidal shapes or fragile textures that would easily fall apart during recycling; White and Houghton, 2006). Identifying primary juvenile clasts in the ash fractions is difficult and was not the focus of this study, which centers on emplacement of the deposits. It is important to keep in mind that most of the phreatomagmatic explosions that excavated Ubehebe Crater were likely fairly shallow, between the ground

surface (top of the fanglomerate) or, perhaps, the lower portion of the S-scoria cone, and the final crater bottom. Deeper explosions may have contributed to an unexposed sub-crater diatreme structure but probably relatively little to the ejecta now distributed around the crater (e.g., Valentine and White, 2012; Valentine et al., 2014). This opening of a crater by excavation, coupled with recycling and removal of original country rock from below the original ground surface, is different from many volcanic craters, which are constructional features formed by the accumulation of material erupted from a vent at the bottom of the crater. Field and experimental evidence indicate that most of the ejected material would have originated above each phreatomagmatic explosion during formation of a maar such as Ubehebe Crater (Valentine, 2012; Lefebvre et al., 2013; Graettinger et al., 2014). Thus, a significant proportion of the basalt clasts in the Ubehebe Crater deposits may be recycled from earlier eruption phases, especially S-scoria, or from early explosions at the crater itself, and these would have played the same thermally passive role as accessory lithic clasts in an individual explosion that emplaced them in a deposit. Such clasts could be considered juvenile on the scale of the entire volcanic center's eruptive episode, but not from the perspective of the final Ubehebe Crater-forming activity that is the focus here. Despite accepting that some proportion of basalt clasts were, like pre-eruption lithics, thermally passive clasts at the time of emplacement, the clasts that we separately identify as "lithic" are those consisting of disaggregated sandstone, pebbles, cobbles, and boulders from the fanglomerate country rock. There is no evidence of fragments from deeper in the local stratigraphy.

Methods

Most of the descriptions and sample collection were completed during four field sessions totaling ~40 days. Seventy-nine sites, representing a range of distances from the crater and topographic settings, were documented in detail, both at natural outcrops and at hand-dug pits (Table A1), and numerous others were subject to briefer observations. Data collection in the field included: descriptions of

stratification and cross stratification, overall grain size and maximum basalt and lithic clast sizes, thicknesses of layers and packages of similar strata, rough proportions of lapilli and block types and their shapes, estimated vesicle content and size in basalt lapilli, internal textures of beds such as clastsize grading, characteristics of contacts between strata and packages of strata, and lateral variations within strata. Reported maximum clast sizes are the average of long-axis dimensions of five large clasts within a horizon at a site and are reported for basalt (MB) and for lithic clasts (ML). Sites were also documented with both sketches and photographs. Samples were collected from individual layers or bed sets, and from consistent intervals within horizons from site to site; a small number of "trench" samples were collected by taking a single sample through an entire section, although this was only practical where deposits totaled ~1 m or less in thickness.

Grain-size analyses were conducted in the laboratory by dry sieving using standard one-o intervals from 4ϕ to -4ϕ (1/16–16 mm). The 1-mm and 2-mm fractions were further analyzed for componentry, first by washing each sample and drying it in an oven, and then by hand-picking individual clasts under a binocular microscope. Clasts were identified as basalt, lithic (country rock), free-quartz grains, and free-feldspar grains. Clast proportions (approximating volume fractions) were computed after counting and separating 200 grains. Many samples were re-analyzed by two to three different workers, counting different splits of samples, and compared, building confidence that the component fractions are robust. Because lithic and free-guartz and felspar grains in the ash fractions are all derived from the host rock of the crater (Miocene fanglomerate), we present the componentry data simply as volume percentage basalt.

STRATIGRAPHY, GRAIN SIZE, COMPONENTRY, AND FACIES DEFINITIONS

Stratigraphy

The stratigraphic sequence of the Ubehebe Crater deposits depends upon distance from the crater

and the local topography. This section focuses on overall characteristics of the deposits and how they vary with distance, which provides a framework for detailed observations at the local scale and facies interpretations.

Proximal

East Gulch site U19-9/U21-4, which is 580 m southeast of the crater center (150 m from the rim), provides the most proximal exposures (note that there is nearly 100% exposure of proximal deposits inside the crater rim, but these are not safely accessible for study). Here, the deposits approach 17 m thick and rest directly on the well-sorted S-scoria fallout (Figs. 2 and 3A). About 50% of the total thickness is composed of beds dominated by basalt and lithic lapilli and block-sized lithic clasts set in a matrix of coarse ash to fine lapilli (Fig. 3B). Individual bed thicknesses are typically several decimeters, up to ~1.5 m, and range from massive to crudely stratified as defined by variations in the proportion of matrix to coarse material and by lapilli and block sizes. These coarse beds are referred to herein as lapilli- and block-dominated beds (LBD). Basalt average maximum clast sizes are in the range of 1-3 cm, and the clasts are subangular with variably abraded surfaces, generally poorly vesicular (<20 vol%), and contain abundant groundmass crystals. Fluidal basalt clasts are very rare; only one small, highly vesicular and fragile bomb, which may be a primary juvenile clast, was found at this site. Lithic clasts are subangular to rounded, and are all derived from the fanglomerate that hosts Ubehebe Crater; average maximum lithic sizes at this station range from 3 cm to 15 cm, but larger, isolated blocks up to several decimeters in size are scattered in the outcrops. Bottom contacts of lapilli- and block-dominated beds sometimes have minor load structures into interbedded, finer-grained horizons, but individual block sags were not observed.

An additional ~30% of the total proximal thickness is composed of thinly bedded lapilli tuff (TBLT; Figs. 2 and 3C). The deposits consist of 2–5-cm-thick, plane-parallel beds of lapilli that range from being framework supported with minor coarse ash to having a supporting matrix of ash. These alternate

with 1-3-cm-thick ash beds that commonly show faint internal cross stratification; together, the beds make a series of couplets with coarse-grained bases and finer-grained upper portions. Fanglomerate-derived pebbles, cobbles, and subangular sandstone blocks are scattered throughout thinly bedded lapilli tuff horizons, but basalt lapilli are generally 1 cm or smaller in size. Sag structures associated with blocksized clasts are crudely developed in some cases but are mostly absent in thick sequences of thinly bedded lapilli tuff at this site. Thinly bedded lapilli tuff horizons are most abundant between lapilli- and block-dominated beds in the lower 3/4 of the section. Thinly bedded lapilli tuff horizons typically do not extend beyond ~700 m from the crater center in most sectors around it, although they occur as far as ~1 km to the north-northwest.

Laminated and cross-laminated (LXL) ash horizons are interstratified with the coarser-grained deposits described above, but they are increasingly abundant in the upper 1/4 of the exposure (Figs. 2 and 3D). These horizons are characterized by dominantly medium ash that forms millimeter-scale laminae, with less abundant coarse- and fine-ash laminae. Bed forms range from plane-parallel to wavy and cross-laminated. Very fine-ash laminae, where they occur, are ~5–10 mm thick and commonly cap or mantle cross-laminated horizons. In some cases, their tops are deformed by tiny sag structures where coarse ash grains or fine lapilli were deposited on top of the very fine ash (e.g., Fig. 3E).

A final type of deposit at this proximal site is massive beds composed of a fine- to medium-ash matrix and scattered coarse ash to medium lapilli and rare blocks (Fig. 3E). These beds are referred to as massive lapilli ash/tuff (MLT) and are most abundant in the upper 1/4 of the sequence. Individual MLT beds here are 10–25 cm thick. Coarse lapilli and isolated blocks within MLT beds are fully contained within the massive ash matrix and do not exhibit sag structures either on the top of the host bed or into underlying deposits (e.g., Fig. 3E). As with very fine-ash laminae in LXL, the tops of MLT beds are locally penetrated by small lapilli associated with overlying deposits.

The site described above (Fig. 2) is a rare proximal location along East Gulch, where the Ubehebe deposits are nearly flat-lying at a confluence of a

small side drainage. Prior to the eruption, East Gulch was a steep-sided channel cut into the fanglomerate substrate. In most locations near the U19-9/U21-4 site, Ubehebe deposits rest on a steep and irregular contact that represents the paleosurface (Fig. 3F); this contact dips toward the channel, with local angles of up to ~40°. Basal Ubehebe deposits share that dip, but the beds approach horizontal upward in the sequence. One potential interpretation is that the deposits were moist and cohesive, allowing them to stick to steep surfaces, but much of the sequence here is composed of lapilli- and block-dominated beds and thinly bedded lapilli tuff deposits, which are coarse-grained and unlikely to have been cohesive. We conclude that in this proximal area, it is more likely that deposits of early explosions were buried before they could remobilize, and deposits from subsequent explosions progressively draped the topography (thinner over highs, thicker in lows), eventually nearly filling the channel. A slight depression above the original channel axis, due to a combination of incomplete filling and differential post-emplacement compaction, caused re-establishment of the drainage and removal of most channel-axis deposits.

Lapilli- and block-dominated beds and thinly bedded lapilli tuff horizons thin rapidly away from the crater. At stations in gulches ~150 and 300 m to the east of U19-9/U21-4, the total thickness of Ubehebe deposits decreases to ~7 m and ~5 m, respectively. This is due to thinning and/or disappearance of lapilli- and block-dominated beds and thinly bedded lapilli tuff horizons. The lapilli- and block-dominated beds observed at Station U19-9/21-4 thin northward in East Gulch and in some cases transition to lenticular layers (see medial station description below; Fig. 2); otherwise, they are not present farther than ~500–600 m from the crater center in East Gulch.

Medial

Site U19-4/U21-3. This site is 650 m from crater center (320 m from the rim), in the lower portion of East Gulch, where it begins to transition to an alluvial fan and topography is more subdued than

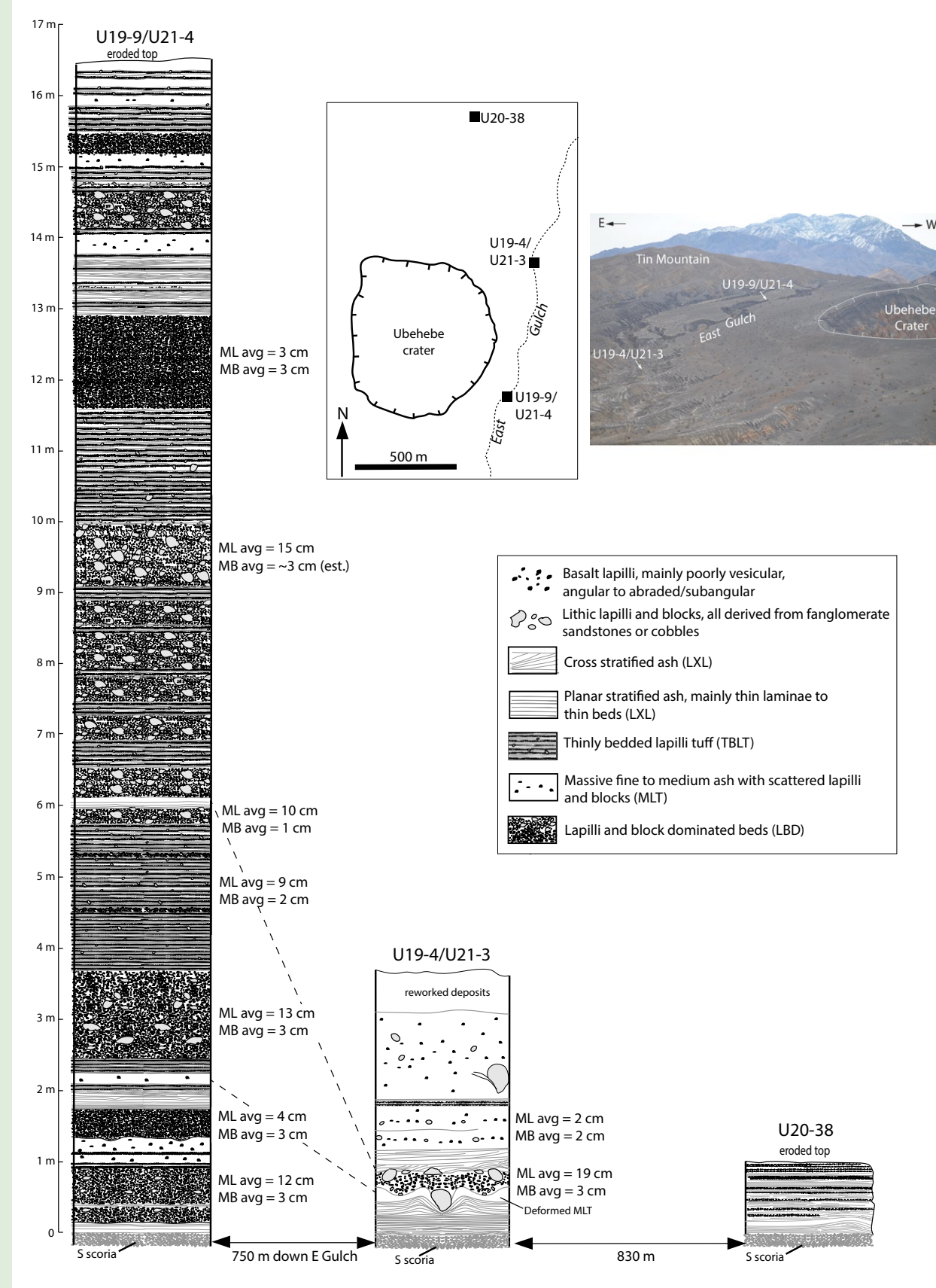


Figure 2. Stratigraphic columns of a proximal site (U19-9/U21-4) and two medial sites (U19-4/U21-3 and U20-38) are shown. Dashed lines show likely correlations among two of the sites, which were determined by tracing horizons along nearly continuous outcrops in the side of East Gulch. Insets show simple location map and a photograph from the north illustrating the relationship between Ubehebe Crater and the two sites in East Gulch. ML—average maximum lithic clasts; MB—average maximum basalt clasts.

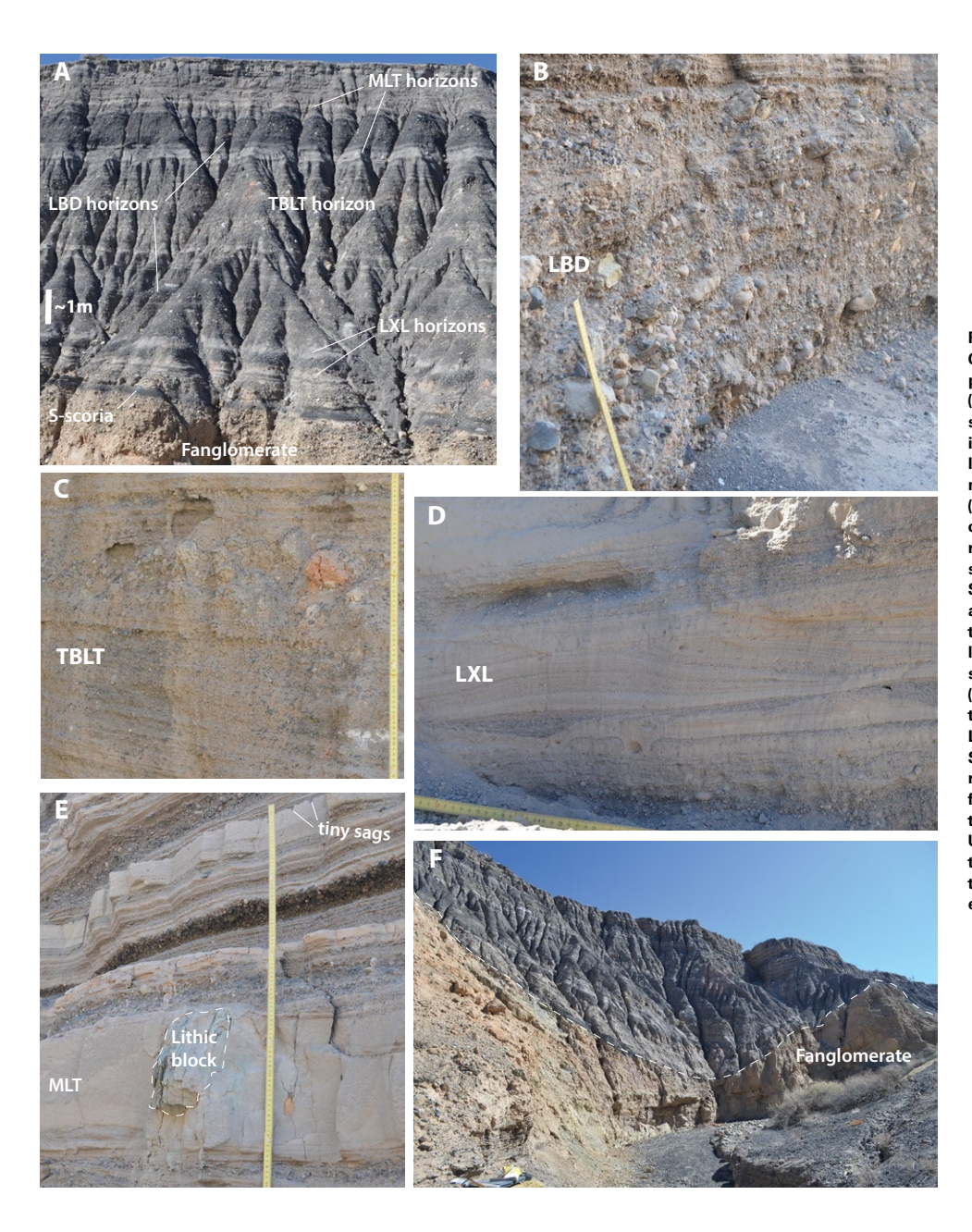


Figure 3. Photographs show proximal Ubehebe Crater deposits exposed in East Gulch. Those in panels A-E were taken at Station U19-9/U21-4. (A) Entire sequence exposed across gulch from station. Examples of laminated and cross laminated (LXL), thinly bedded lapilli tuff (TBLT), lapilli- and block-dominated (LBD) beds, and massive lapilli tuff (MLT) horizons are indicated. (B) Detailed view of a typical LBD bed, in this case internally crudely stratified. Cobbles derived from fanglomerate and basalt lapilli are supported by a matrix of coarse ash to fine lapilli. Scale is 40 cm. (C) Example of stratified coarse ash-fine lapilli interbedded with an ~20-cmthick, massive LBD layer (containing orange lithic clast). Scale is 60 cm. (D) Dune and cross stratification in LXL horizon. Scale is 20 cm. (E) Examples of MLT bed interbedded with LXL, thinly bedded lapilli tuff, and decimeter-thick LBD horizons near top of proximal sequence. Scale is 80 cm. (F) Nearby exposure shows irregular contact between Ubehebe deposits and fanglomerates. The contact dips upward from the channel axis at ~40°. Near the top of the Ubehebe deposits, the beds are near horizontal, illustrating rapid filling and smoothing of the steep channel, which was subsequently reeroded to form modern exposures.

in the very proximal locations. Ubehebe Crater deposits here lie flat, and the site is near the channel axis. The total thickness of unmodified Ubehebe Crater deposits, which rest upon S-scoria, is 3.2 m (Figs. 2 and 4A); they are capped by an erosional contact that is overlain by a few decimeters of fluvially reworked material. All four facies are present.

The 50 cm of basal Ubehebe Crater deposits at this site are laminated and cross-laminated ash with some coarser layers also containing fine lapilli (Fig. 4B). The lower ~10 cm are fine to medium ash that forms a low-angle dune form that is 30 cm long and 3 cm high. An ~1-cm-thick layer of very fine-ash mantles this and has small-scale load structures from the overlying coarser layer. The upper ~40 cm of this horizon is characterized by plane-parallel, coarse-fine couplets (Fig. 4B). The entire horizon is labeled LXL in Fig. 4A, but the coarser layers approach the characteristics of the thinly bedded lapilli tuff facies described above. The horizon is overlain by a massive lapilli ash/tuff that is up to 25 cm thick but is deformed due to loading by the overlying lapilli- and block-dominated bed (Fig. 4C) This is the only lapilli- and block-dominated bed observed at the site; it is up to 40 cm thick, but its thickness is irregular here, and it grades laterally to a lenticular character. It is the lateral equivalent of one of the lower lapilli- and block-dominated beds described at the proximal site above, and, as at the proximal site, maximum basalt clasts average 3 cm while lithic clasts average 19 cm with the largest block, which rests on the bed's top, at 42 cm. All lapilli and blocks are supported within an ash matrix. Basalt lapilli are similar to those described in proximal lapilli- and block-dominated bed deposits; they are poorly vesicular, subangular, and contain abundant groundmass crystals. The lapilliand block-dominated bed is overlain by 40 cm of ash with prominent low-angle cross lamination; two coarser, 2- and 4-cm-thick, fine lapilli-bearing layers pinch out against dune crests formed by the dominant cross-laminated ash.

With the exception of a 17-cm-thick horizon of thinly bedded lapilli tuff at the 2-m level (Fig. 4D), the upper 1.9 m of Ubehebe deposits at this site are composed of three clearly delineated massive lapilli ash/tuff beds (Figs. 4A and 4E). Basalt lapilli contain

30-50% submillimeter vesicles and are subangular with variably abraded edges; they, along with lithic lapilli, are scattered throughout the MLT beds but have higher concentration in 5-10-cm-thick bands, which gives the appearance of coarse "stringers" on the weathered outcrop surface (see also Crowe and Fisher, 1973). The two lowest MLT beds, which are 32 and 35 cm thick, are separated by a discontinuous, 1-cm-thick coarse ash layer (center of Fig. 4E). The uppermost MLT bed contains a large block, which penetrates the bed and produces a sag structure into underlying strata (Fig. 5). The sag structure includes a highly deformed, laminated and cross-laminated horizon that is absent elsewhere; it is only preserved in the sag structure, and its laminae are truncated by a sub-horizontal contact that laterally forms a subtle (cryptic) contact within the MLT facies. This structure indicates that a LXL horizon was present but, except where protected beneath the block, was stripped sometime between the deposition of two MLT beds. The block was rooted in this LXL horizon rather than in an MLT bed. These features provide important information regarding erosional processes associated with the emplacement of MLT units, which are further detailed in a subsequent section.

Site U20-38. This site is located 1475 m north of the proximal site described above and is 1120 m north of crater center (800 m from the rim). Ubehebe Crater deposits here are 1 m thick and composed entirely of the laminated and cross-laminated ash facies (Figs. 2 and 6). Four well-developed dune forms were observed (e.g., Fig. 6); these have lengths of 25-60 cm and heights of 2-7 cm. While the bulk of the deposit is composed of laminated and cross-laminated medium-coarse ash, fine ash layers that maintain constant thickness across the exposure are also present (Fig. 6) and are interpreted to represent settling of fine ash from the air between LXL emplacement pulses. Coarsefine couplets are present in the upper 45 cm of the deposit, with the coarse layers being well sorted (based upon visual inspection) coarse ash to fine lapilli and, in some cases, approaching a framework-supported structure. Very fine-ash caps each couplet, and the tops of these strata are penetrated by coarser clasts associated with the overlying

couplets. The coarse basal layer of the uppermost couplet contains scattered, flake-shaped, highly vesicular basalt lapilli that can be correlated in nearby exposures and therefore serve as a local marker layer. These fragile flakes are likely primary juvenile clasts, as they would not have survived recycling processes in the vent area.

Distal

Ubehebe Crater deposits progressively thin with increasing distance to the north and west-northwest of the crater, areas where topography is subdued in comparison to sectors to the east and south. The only facies observed in these deposits is LXL ash; cross lamination gradually disappears with increasing distance so that the deposits become planar parallel-laminated, and in some areas the lamination becomes more poorly defined (Fig. 7). There is little variation in the deposits other than thinning with distance, which gradually reaches ~5 cm at a distance of 9 km from crater center. Because of the similarities, we focus here on general patterns recorded in the distal deposits. Some layers can be correlated from site to site. For example, at U20-39 and U20-40, there are two coarse-fine couplets in the middle third of the deposit, and the coarse lower laminae of these couplets form distinct dark bands. A coarser layer, which includes small basalt and lithic lapilli, occurs higher in the sequence; the relative abundance of lithic clasts in the layer varies but is highest at sites northwest of the crater (Figs. 7A-7C). The coarser layer is found in some of the most distal sites, such as U20-55 (~3000 m from crater center, 10 cm thick; Fig. 7D). It is likely that the two couplets and this coarser layer correlate to the couplets and to the flake-bearing layer described at the medial site above (Site U20-38; Fig. 6).

Grain Size and Componentry

Median grain size and Inman sorting of samples from the facies described are grouped into three fields: lapilli- and block-dominated, thinly bedded lapilli tuff and laminated and cross-laminated ash,

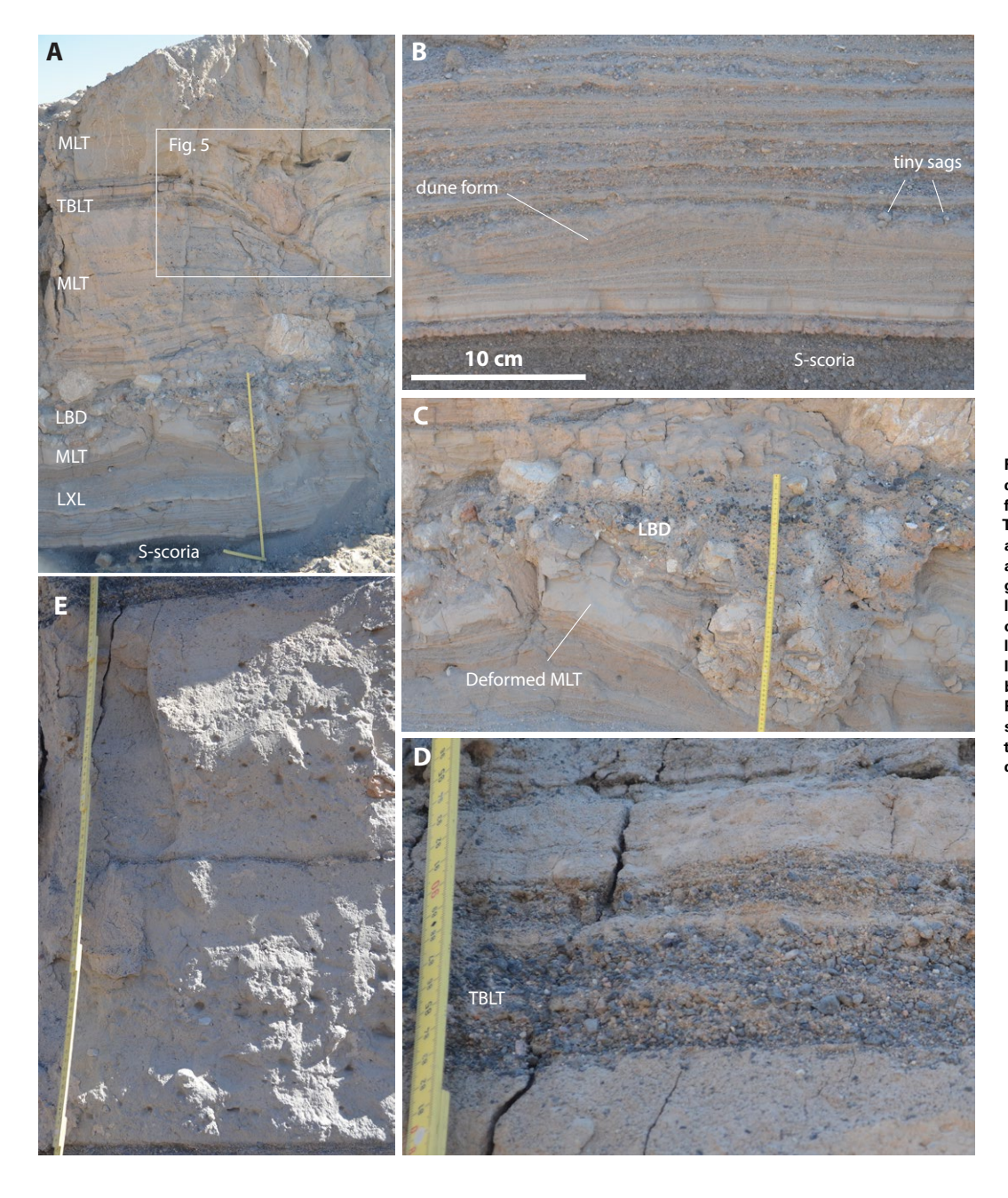


Figure 4. Photographs show deposits at medial site U19-4/U21-3. (A) Entire sequence with facies labeled. MLT-massive lapilli/ash tuff; TBLT-thinly bedded lapilli tuff; LBD-lapilliand block-dominated beds; LXL-laminated and cross-laminated. Ruler is 1 m long. Rectangle outlines area detailed in Figure 5. (B) Lower laminated and thinly bedded horizon. (C) Detail of lapilli- and block-dominated bed, including load-induced deformation of underlying massive lapilli tuff. Ruler is 50 cm. (D) Detail of thinly bedded lapilli tuff in upper portion of sequence. Ruler is ~15 cm. (E) Two massive lapilli tuff beds separated by 1 cm coarse ash layer. Indentations are locations of lapilli that were dislodged during outcrop preparation. Ruler is ~70 cm.

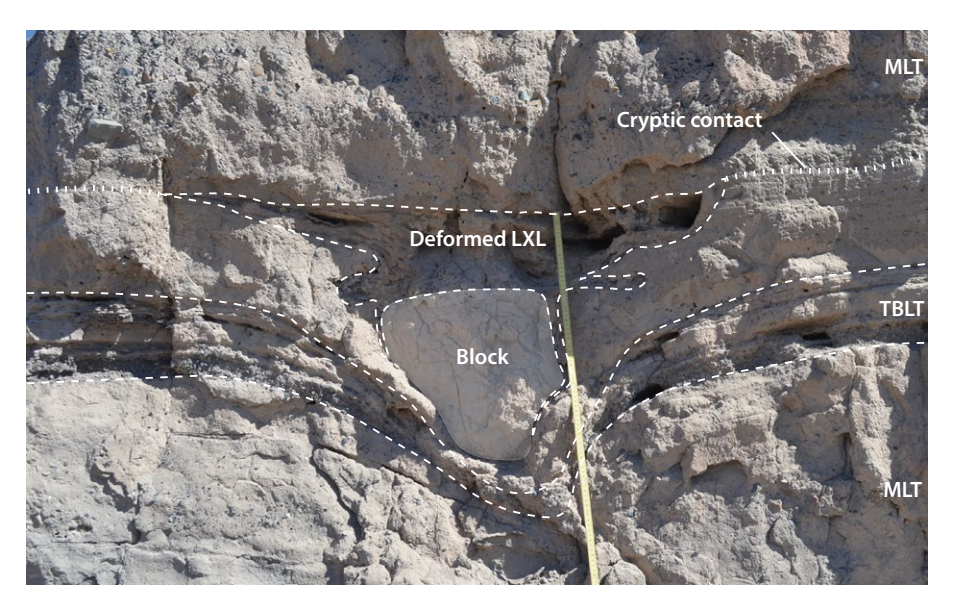


Figure 5. Detail shows preservation of otherwise missing laminated and cross-laminated (LXL) horizon in a block sag structure and truncation of the horizon by a subhorizontal contact that extends laterally into a cryptic contact (dotted line) between two massive lapilli/ash tuff (MLT) beds with slightly different grain sizes. TBLT—thinly bedded lapilli tuff.

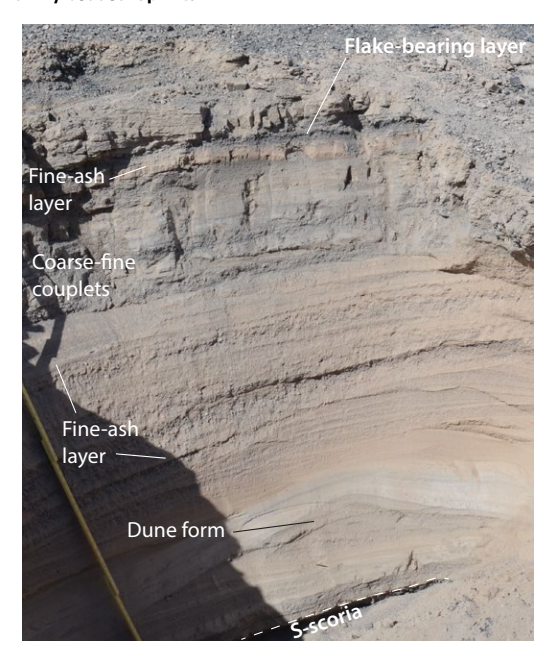


Figure 6. Photograph of deposits at medial site U20-38 is shown. Entire sequence is laminated and cross-laminated ash. Thin layers containing coarse ash and fine lapilli are the coarse portion of coarse–fine couplets. The uppermost of these contains scattered fragile, highly vesicular, flake-shaped basalt lapilli up to 2 cm in size, which facilitates correlation of units at nearby sites. Fine-ash layers, ~0.5–2 cm thick, are interstratified in the deposits; three examples are highlighted in the photo. These maintain constant thicknesses across the exposure.

and massive lapilli tuff (Fig. 8). Most lapilli- and block-dominated beds are too coarse to adequately sample for laboratory sieve analysis, but the few samples that were collected, which can be considered to represent matrix material rather than entire beds, have median grain sizes of 1-4 mm and Inman sorting values of $\sigma_{\phi} \approx 2$ (Fig. 8). In keeping with the lithic-rich nature of lapilli- and block-dominated beds observed in the field, component analysis of the 1 mm size fraction shows that the samples are skewed toward lower basaltic ash (higher lithic) contents than the distribution for all samples (Figs. 9A and 9B). Median diameters of thinly bedded lapilli tuff samples are ~1-2 mm (see the coarser samples of LXL/thinly bedded lapilli tuff field in Fig. 8), while LXL median diameters are mostly in the range of 1/8-1/2 mm, and σ_{ω} is between 1 and 2 for most samples. Note that most of these samples include material from multiple layers or laminae. Grains in the LXL 1 mm size fraction are typically 60-90 vol% basaltic ash (Fig. 9C). The basaltic ash grains are mainly poorly to moderately vesicular, angular to subangular, and variably abraded. MLT deposits share grain-size characteristics with the majority of LXL samples (Fig. 8), although a few are more poorly sorted than LXL/thinly bedded lapilli tuff due to the presence of small percentages of coarse lapilli. Clast types in the 1 mm fraction of MLT samples are similar to LXL/thinly bedded lapilli tuff but skewed toward higher basaltic ash content, with nearly half of samples having 80-90 vol% basalt (Fig. 9D).

Distribution of deposits to the north-northwest and west of the crater can provide information on proximal to distal variations in granulometry without significant local topographic influences. To the west, thickness decreases from ~5.1 m at 780 m distance to 37 cm at 1990 m, while median diameter generally becomes finer (but with significant scatter) and sorting remains roughly constant (Figs. 10A–10C; note that grain-size data are for samples that include multiple laminae in the case of LXL). Similarly, to the north-northwest, thickness decreases from ~3.2 m at 650 m from crater center to 10 cm at 3 km (Fig. 10D). Median diameter does not show systematic change over that distance, and sorting tends to become poorer (but with significant

scatter; Figs. 10E-10F). The main facies type in both directions is LXL (minor thinly bedded lapilli tuff in the two most proximal sites plotted) except in the two thickest sites plotted, which also include some MLT beds. The most proximal site described above (17-m-thick site U19-9/U21-4) is not plotted here due to the coarseness of many of its layers; grain-size parameters measured in the lab would not be representative of deposits in that section.

■ FACIES INTERPRETATIONS AND LOCAL CHARACTERISTICS

In this section, we focus on each of the facies types. We begin with a broad interpretation of emplacement for each facies, which provides context for the presentation of additional data and the details they reveal.

Lapilli- and Block-Dominated Facies

There are two potential interpretations for emplacement of the proximal lapilli- and blockdominated beds: fallout and ballistic curtain. Fallout from buoyant eruption columns is unlikely for two reasons. (1) Development of most buoyant columns depends upon effective heat transfer between abundant ash-size, primary-juvenile clasts, and the gas phase (e.g., Sparks et al., 1997). Many of the lapilli- and block-dominated beds are rich in

lithic clasts derived from country rock that would likely have been relatively cool, and by definition the beds are dominated by particles coarser than ash. Proportions of basalt and lithic clasts observed at the outcrop vary; the 1-mm sieve fractions of most samples contain between 30 vol% and 50 vol% lithic grains, which is more than in samples from other types of Ubehebe deposits (Figs. 9A) and 9B). Demonstrably primary juvenile material, which would be a source of heat in driving buoyant eruption columns, is rare. It seems possible that many of the basalt clasts in the deposits are recycled to some degree (for example, from the early S-scoria cone that was disrupted by Ubehebe Crater), and they may have been relatively cool when ejected. As a result, we expect that ejected

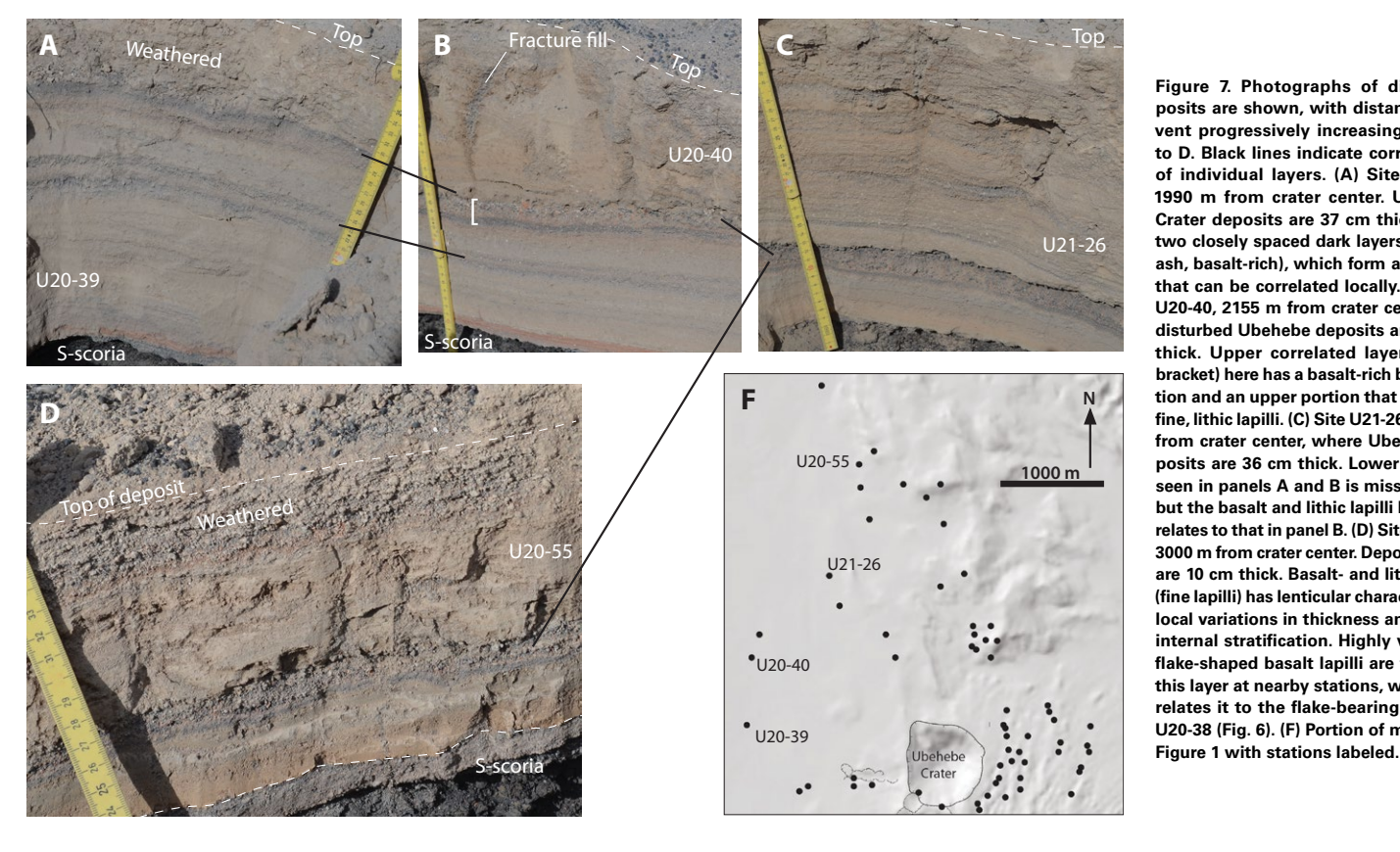


Figure 7. Photographs of distal deposits are shown, with distance from vent progressively increasing from A to D. Black lines indicate correlations of individual layers. (A) Site U20-39, 1990 m from crater center. Ubehebe Crater deposits are 37 cm thick. Note two closely spaced dark layers (coarse ash, basalt-rich), which form a doublet that can be correlated locally. (B) Site U20-40, 2155 m from crater center. Undisturbed Ubehebe deposits are 37 cm thick. Upper correlated laver (white bracket) here has a basalt-rich basal portion and an upper portion that is rich in fine, lithic lapilli, (C) Site U21-26, 2115 m from crater center, where Ubehebe deposits are 36 cm thick. Lower doublet seen in panels A and B is missing here, but the basalt and lithic lapilli layer correlates to that in panel B. (D) Site U20-55, 3000 m from crater center. Deposits here are 10 cm thick. Basalt- and lithic layer (fine lapilli) has lenticular character with local variations in thickness and vague internal stratification. Highly vesicular, flake-shaped basalt lapilli are found in this layer at nearby stations, which correlates it to the flake-bearing layer at U20-38 (Fig. 6). (F) Portion of map from

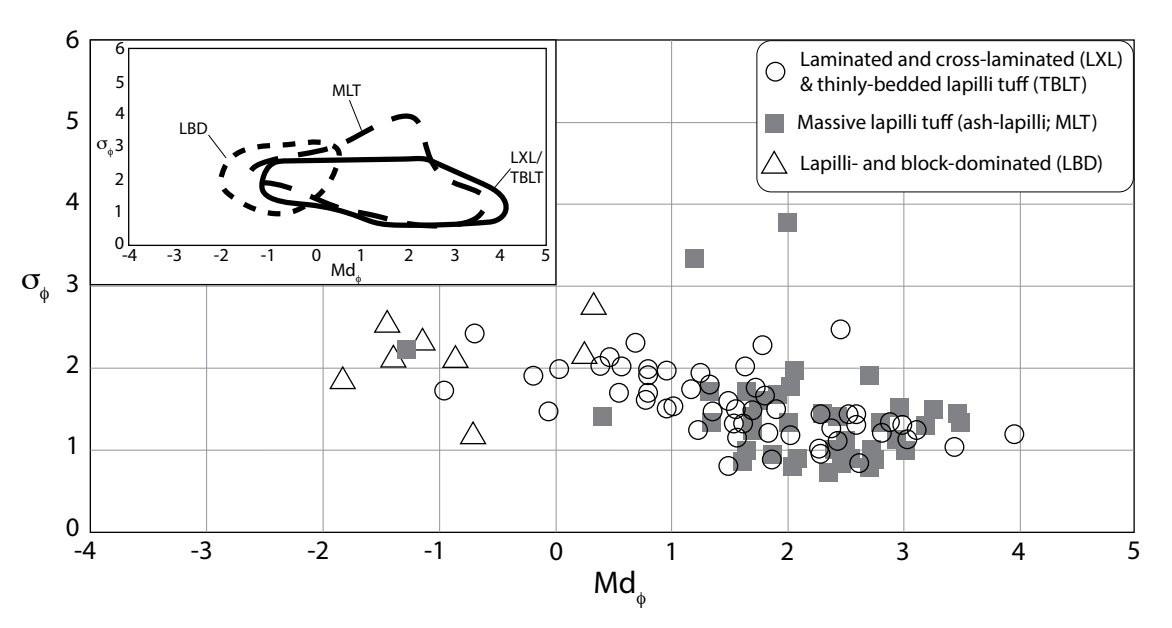


Figure 8. Inman sorting (σ_•) and median diameter (Md,) are plotted for samples of the three main facies types formed by Ubehebe Crater eruptions (see Fisher and Schmincke, 1984). Most of the laminated and cross-laminated (LXL) ash and thinly bedded lapilli tuff (TBLT) and massive lapilli ash/tuff (MLT) samples fall within a field similar to that documented by Crowe and Fisher (1973). Inset shows the fields occupied by each of the three facies. Note that LXL and MLT samples are representative of the bulk deposits, but the lapilli- and block-dominated (LBD) bed samples only represent the matrix of the coarse deposits.

gas-particle mixtures probably did not contain sufficient hot ash to support the formation of buoyant eruption columns that would produce thick fallout deposits. (2) The limited lateral extent of continuous lapilli- and block-dominated beds, and the common observation that maximum lithic sizes are much larger than maximum basalt clasts even though their assumed densities are similar (poorly vesicular basalts compared to sandstone and metamorphic clasts), seems inconsistent with fallout from a buoyant plume and potential umbrella cloud, although it is possible that this fact is related to the basalt clast sizes that were available for dispersal.

We favor an interpretation that these coarse proximal beds were deposited by ballistic processes. The lapilli- and block-dominated beds are analogous to facies described for experimental ballistic curtains, which form sheet-like deposits in radial directions but also rays that result in variable thickness in the circumferential direction (Graettinger et al., 2015a, 2015b). As with experiments, ballistic curtain deposits grade outward into clusters of large clasts and eventually to isolated clasts. Lapilli- and block-dominated bed deposits

at the medial site U19-4/U21-3 (Figs. 4A and 4C), ~650 m from the crater center, record this transition. Isolated ballistic clasts that produced sag structures into previously emplaced, finer-grained deposits are common throughout the Ubehebe Crater deposits within ~1 km of the crater center, and we note that continuous beds of up to ~20 cm thick extend to 1 km distance from the north of the crater and radially outward from the lowest portion of its rim. As mentioned in the Introduction, explosion within a crater may produce inclined and/or collimated jets and localized clast showers. This type of ballistic deposition may also have produced some of the lapilli- and block-dominated beds around Ubehebe Crater.

Laminated and Cross-Laminated Ash and Thinly Bedded Lapilli Tuff

Interpretation

We interpret both thinly bedded lapilli tuff and laminated and cross-laminated ash to have been deposited directly by pyroclastic surges. Thinly

bedded lapilli tuff is most common in proximal areas where the surges carried coarser clasts. Coarse-fine couplets likely each represent a pulse of pyroclastic surge at a given location (see also Vazquez and Ort, 2006), which may be related to individual explosions in the crater or to transient flow phenomena unrelated to the source, such as pulses that were diverted by topography. The coarse layers record rapid sedimentation of large particles from the suspended load during the waxing or high-speed initial part of a pulse. Coarse ash grains and lapilli in the coarse layers commonly formed tiny sag structures into many underlying fine-ash layers (deposited at the end of preceding pulse), which indicates mainly vertical sedimentation onto a powdery bed rather than substantial lateral motion as in a bed load. The upper, finer layers of couplets represent more gradual ash sedimentation during pulse waning, with well-developed bed loads that produced both planar parallel and cross lamination.

Coarse–fine couplets are also observed in medial and distal locations (Figs. 6 and 7), but at these distances the coarse layers are medium ash to fine lapilli, while the fine horizons are mainly

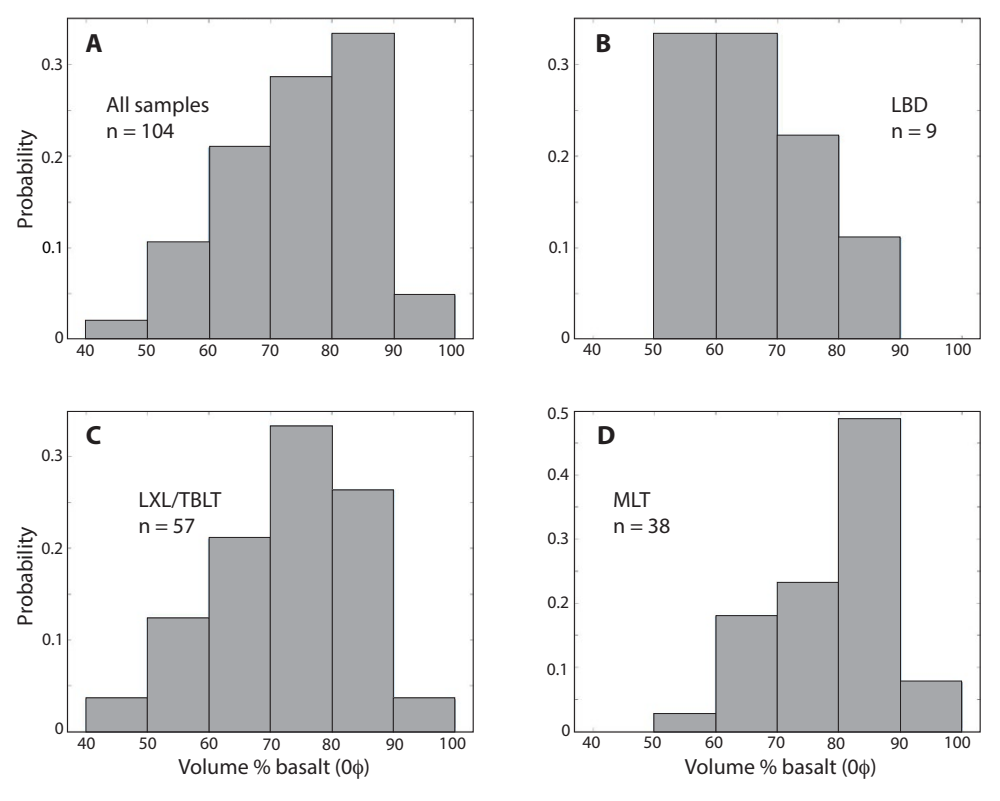


Figure 9. Graphs show the proportion of basalt clasts in the 1 mm size fraction of Ubehebe deposits (based upon clast counts, approximating volume fractions). All other components (lithic and free-quartz and feldspar crystals) are derived from the fanglomerate country rock. (A) All samples. (B) Lapilli- and block-dominated (LBD) matrix samples. Basalt content in this fraction is skewed toward lower values of 50-60 vol%. (C) Laminated and cross-laminated (LXL)/thinly bedded lapilli tuff (TBLT) ash deposits, where ~2/3 of samples contain 70-90 vol% basalt in the 1 mm fraction. (D) Massive lapilli ash/tuff (MLT) deposits, which are skewed toward higher basalt contents.

fine to medium ash. Very fine-ash laminae that cap or mantle bedforms or coarse-fine couplets likely represent the settling of remaining fine particles after a pulse of pyroclastic surge. In some places, there is ambiguity as to whether a given coarse layer is best interpreted as a separate fallout deposit rather than as part of a surge pulse. For example, near the top of the Ubehebe deposits north of the crater, the 1.5-2-cm-thick coarse layer of a couplet contains scattered, flake-like, fragile basalt lapilli (site U20-38, also see above; Fig. 6) that seem unlikely to have been able to survive extensive transport in a pyroclastic surge. Flakes are present in this layer at sites within ~300 m of U20-38. Farther north, the layer is 2.5 cm thick and dominated by basaltic coarse ash to fine lapilli, some of which are highly vesicular but not flake-shaped. Between 650 m and 2100 m north of U20-38, the layer is reverse-graded with coarse ash in its upper portion and with faint lamination in its lowest centimeter, but basalt clasts are subangular, and no flakes were observed. At sites northwest of the crater, a correlated layer is typically 2-2.5 cm thick, has a basalt-rich coarse ash base, a slightly finer middle, and an upper part with fine lapilli, of which 20-30% are lithic clasts (Fig. 7B). It is possible that our correlations are incorrect, although the consistency in stratigraphy at the different sites lends confidence to them. These observations indicate that the fragile basaltic flakes only are found in the layer within a limited area, and that elsewhere the layer has variable thickness, lithic content, internal grading, and in some cases faint lamination. Uncertainty remains as to whether this coarse layer was emplaced by fallout from a buoyant eruption column as opposed to rapid, suspended load sedimentation during the initial part of a surge pulse, but we favor the latter. The fragile, flake-like clasts may represent primary juvenile clasts that were ejected during the surge-producing explosion (see White and Valentine, 2016) and followed different trajectories and fell through the surge as it passed across the area where the flakes are found.

The observation that LXL horizons are most abundant in the upper 1/4 of the proximal site (Fig. 2) may reflect progressive deepening of the crater, which vertically focuses or collimates an explosion jet as mentioned above. After rising to their maximum heights, many such jets collapse straight down and rapidly deposit poorly-sorted material onto the crater floor. This rapid sedimentation can expel interstitial gas and fines from the base of the jet, which in turn become fine-grained lateral density currents (pyroclastic surges; Valentine et al., 2012, 2015, 2017; Taddeucci et al., 2013; Graettinger et al., 2015a).

Pyroclastic Surge Properties and Bed Forms

Ubehebe Crater deposits, particularly within ~700 m of the crater center, consist of many layers of different types, including lapilli- and block-dominated beds, thinly bedded lapilli tuff, and horizons of laminated and cross-laminated ash. All of these are consistent with the crater and its ejecta being the result of a large number of explosions that distributed particles by ballistic processes (in lapilli- and block-dominated beds) and density currents (thinly bedded lapilli tuff, LXL). The

density currents (surges) were mainly impulsive rather than sustained, as indicated by repeated coarse–fine couplets; in some ways, the deposits are similar to a sequence of small-scale lateral blast deposits (e.g., Belousov et al., 2007; Breard et al., 2015), but the blasts were not necessarily inclined

or laterally directed (see also Valentine, 2012). This reduces or eliminates the applicability of classical sediment-transport analysis, such as was applied by Valentine (1987), Dioguardi and Dellino (2014), and Dellino et al. (2021), which is originally based upon theory and experimental data for steady,

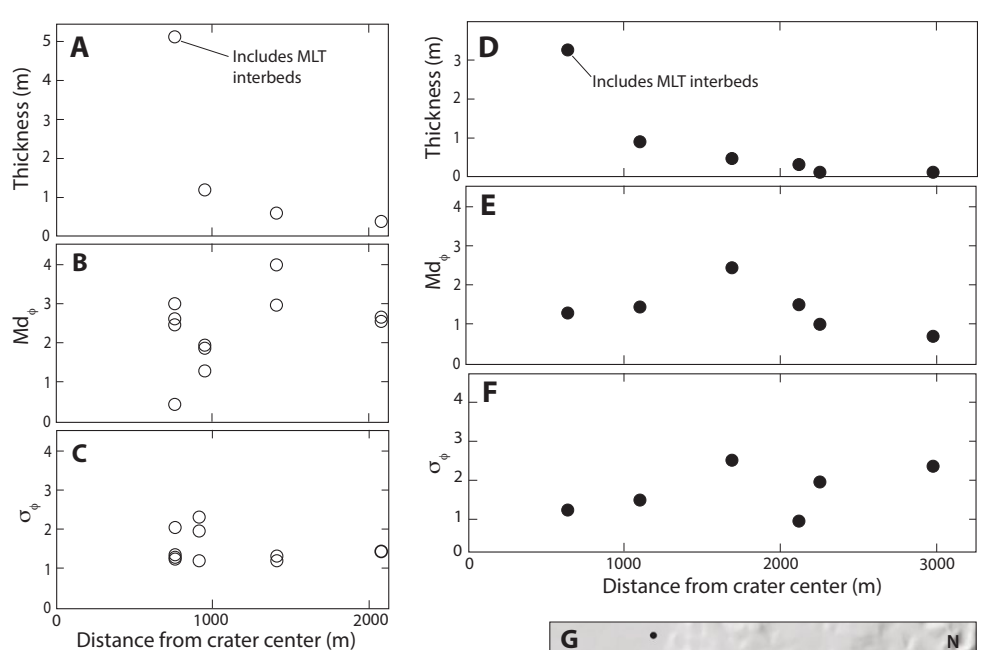


Figure 10. Proximal-to-distal variations of Ubehebe Crater deposits as functions of distance from crater center in directions where topographic variations are relatively subdued. (A–C) Thickness, median diameter (\$\phi\$-units), and Inman sorting to the west of the crater. (D–F) Thickness, median diameter (\$\phi\$-units), and Inman sorting north of the crater. (G) Location map, with labeled sites corresponding to data plotted in panels A–F. Relatively proximal sites include massive lapilli ash/tuff (MLT) beds in total thickness, while other sites only contain laminated and cross-laminated deposits.

uniform flows rather than flows with strong accelerations and decelerations over short time frames (e.g., Middleton and Southard, 1978). Similarly, the classical theory is based on flow down an inclined plane, a condition that is violated in eastern and southern quadrants around the crater due to the rugged topography. For these reasons it is necessary to apply a transient, three-dimensional flow model to constrain conditions such as velocity and sedimentation rate that are implied by deposits at a given location; work is underway to address this, but it is outside the scope of this paper.

Dune forms are common in the laminated and cross-laminated facies within 2 km of Ubehebe Crater and have a variety of characteristics (Fig. 11). In most cases, a dune rests on planar laminae that are roughly parallel to the paleosurface. The base of a dune is marked by a localized swelling of a lamina or very thin layer, above which a dune form amplifies. In some cases, many laminae within a dune are relatively continuous from stoss to lee limbs (e.g., Fig. 11A), while in others that show downslope migration, the lee-side (foreset) laminae are truncated by the final dune surface (Fig. 11B). Dune migration directions are typically parallel to and down the paleoslope (see also Crowe and Fisher, 1973), whether in a channel or on an open slope, but at any given location it is also common to see some up-slope migration (e.g., Fig. 11C). Examples in East Gulch (Figs. 11A-11C) show mainly downslope migration, with some up-slope, but in all of the cases we observed, migration is parallel to the channel axis even though it is approximately orthogonal to the radial direction from crater center. The migration directions in channels indicate that the lower portions of pyroclastic surges were blocked and diverted by local topography (e.g., Valentine, 1987). Our dune-form dimensions data (Table 1) are consistent with those of Crowe and Fisher (1973). Lengths are commonly ~30-90 cm, but some longer ones, up to 2 m, were measured (e.g., Fig. 11D). We did not observe a systematic change in dune size with distance from crater. The lack of systematic trends and the variability within individual vertical sections suggests that the dune forms were emplaced from a number of different pyroclastic surges with different transport

OU20-39

U20-63

U20-64^O

U20-55

U20-34

U20-33

U21-26

U20-49

U20-48

1000 m

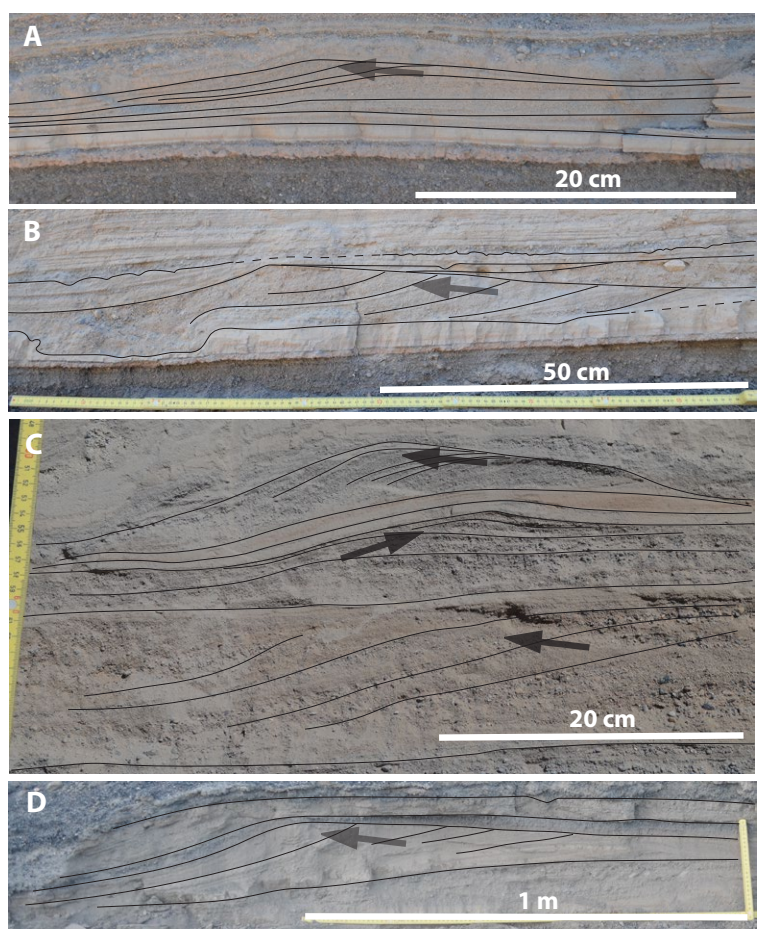


Figure 11. Dune forms in laminated and cross-laminated ash are shown. Contacts between some laminae are marked with thin lines to illustrate cross stratification. Gray arrows indicate dune-crest migration. Sites shown in panels A-C are in East Gulch, while that in D is west of the crater. (A) Very low-angle, low-profile dune formed by progressive local thickening of laminae over an initially flat bed. Migration direction is to left (north), down-channel. Site U19-4/U21-3, 650 m northeast of crater center. (B) Dune form with foreset laminae truncated by dune surface. Migration is to left (north), down channel. Site U19-6, 620 m east of crater center. (C) Three examples of cross-stratification over a small vertical distance in an outcrop. Lower portion shows foreset beds that accumulated from right to left (down channel, northward), but surface of dune was truncated. Middle dune migrated left to right (southward, up channel) and is overlain by a third dune form with a left-migrating crest (northward, down channel). Site U19-5, 630 m northeast of crater center. (D) Dune form with length of ~2 m, crest migration to left, westward and down a paleoslope. Site U20-32, 960 m west of crater center.

properties at a given location and in different sectors around the crater.

Crowe and Fisher (1973) noted the low angles of stoss and lee limbs of dune forms, compared to an angle of repose of around 30°, which we also observed (Table 1), and pointed out that many dune forms resemble the forms of climbing ripples (a.k.a. ripple-drift cross lamination), albeit with larger wavelengths and heights than those of many fluvial or coastal climbing ripples. In fluvial systems, climbing ripples are attributed to unsteady transport of sediment-rich water with simultaneous sedimentation from suspended loads and bed loads (e.g., a crevasse splay), which is somewhat analogous to deposition from transient pyroclastic surges (see also Douillet et al., 2013). The angle of climb (α) in climbing ripple-like bed forms is defined as the angle from dune-form crest to the overlying crest(s), measured relative to dip of a planar bed upon which a dune has formed. Allen (1970a; see also Allen, 1970b, Chapter 2) suggests that the angle of climb is proportional to the ratio of mass flux of sediment delivered from suspension to the bed load, to the bed-parallel sediment flux in the bed load (in this case, the sediment carried within the "bodies of the ripples" as they move along the bed; Allen, 1970a):

$$\tan \alpha = \frac{MH}{2j_b}.$$
 (1)

Here H is the height of the ripple or dune. M (kg/m2.s1) is the mass aggradation rate of the bed, i.e., the rate at which mass accumulates from suspended load onto the bed with a bulk density $\rho_b =$ $(1-\varepsilon)\rho_{p}$, where ε is bed porosity and ρ_{p} is the particle material density. In other words, $M = v_b \rho_b$ where v_b is the rate of deposit thickening (m/s). $i_b(1/2H)^{-1}$ is the horizontal sediment mass flux through a unit cross-sectional area of the ripple measured perpendicular to the transport direction (i_b has units of kg/m·s), assuming idealized triangular ripple cross sections. While we interpret the Ubehebe pyroclastic surge deposits to have been produced by highly transient flows, these parameters are expected to apply during a pulse of sedimentation that produces a climbing dune form. With Equation 1, we can estimate the ratio of suspended load

TABLE 1. DUNE-FORM DATA FOR UBEHEBE CRATER DEPOSITS

Site	Distance to crater center (m)	Length (cm)	Height (cm)	Right limb angle (degrees)	Left limb angle (degrees)	Climb angle (α) (degrees)*	Sediment flux ratio [†] (tanα)	Exposure orientation	Comment
U19-4	650	30	3			15	0.28	N-S	Migration to N, downslope away from crater
U19-5	630	43	7	3	22	25	0.47	N-S	Migration to S, upslope toward crater
		53	7	3	18	3	0.05	N-S	Migration to N, downslope away from crater
U19-6	620	96	9	4	22	NA		N-S	Migration to N, downslope away from crater
		105	9.5	5	8	2	0.03	N-S	Migration to N, downslope away from crater
		140	16	3	8	NA		N-S	Migration to N, downslope away from crater
U19-24	730	50	5	12	12	28	0.53	N-S	Migration to N, away from crater and downstream
U20-32	960	200	7	3	24	NA		E-W slope	Migration to W, away from crater
U20-33	790	55	3	11	7	NA		NW-SE	Migration to NW, away from crater and downslope
		75	2.5	8	17	16	0.29	NW-SE	Migration SE, toward crater and upslope
		90	4	12	14	NA		NW-SE	Migration to NW, away from crater and downslope
U20-37	955	31	1.5	0	8	16	0.29	NW-SE	Migration to SE, upslope and away from crater
U20-38	1120	60	7	2	21	22	0.40	N-S	Migration to N, upslope, away from crater
		30	2	1	18	NA		N-S	Migration to N, upslope, away from crater
		25	2	1	22	16	0.29	N-S	Migration to N, upslope, away from crater
U20-63	1390	120	5.5	2	8	NA		E-W	Migration to W, away from crater
U21-9	1300	45	5	8	17	20	0.36	NE-SW	Migration to NE, away from crater and downslope
U21-22	950	30	8	3	22	NA		E-W	Migration to W, away from crater, downslope

^{*}Cases with climb angles had laminae that were continuous across crests; NA indicates that foreset laminae were truncated, and crest-to-crest climb angle could not be determined. †See Equation 1 in text.

sedimentation to the bed-load transport using field measurements of α and H (Table 1). If the model for climbing ripples is correct, the data imply that bed-load fluxes were 2–20 times larger than the sediment flux from suspension during the formation of many dune forms in the LXL facies.

Our estimate of the ratio of sedimentation flux to bed-load flux (0.05-0.5) is similar to that predicted by Dellino et al.'s (2020) surge-bed form regime diagram (~0.02–0.25), where the ratio can be estimated based on dune-form length (in our case, most dune-form lengths are ~30-200 cm; Table 1). The latter estimate is based on a completely different approach that combines classical sediment-transport theory and large-scale experimental data. Using the follow-on work of Dellino et al. (2021, see their fig. 4E), our wavelength data, and Md ≈1-2 (appropriate for most LXL samples; Fig. 8), M was between 5×10^{-4} to 5×10^{-5} kg/m²·s¹. This range of sedimentation flux implies bed-load fluxes of ~10⁻⁴–10⁻² kg/m²·s¹ for the flux ratio based on Allen (1970a) and 2×10^{-4} to $2.5 \times$ 10⁻² kg/m²⋅s¹ for the flux ratio based on Dellino et al. (2020). The similarity of the ratios computed using

Equation 1 and those estimated from the Dellino et al. (2020) work is promising, and the above-mentioned transient flow modeling will test whether the suspended load sedimentation rates from classical sediment-transport theory can be applied to situations such as at Ubehebe.

Massive Lapilli Ash/Tuff Facies

Interpretation

Massive lapilli ash/tuff beds are interpreted to have been deposited by high-concentration, dry granular flows that resulted from the remobilization of pyroclastic surge deposits from steep slopes. Our interpretation is based on the following broad lines of evidence. (1) Grain-size characteristics of MLT beds are generally the same as LXL-thinly bedded lapilli tuff (Fig. 8), but the textures of MLT beds are massive rather than internally stratified, which supports the possibility that MLTs are homogenized versions of the former. (2) MLT beds

are only found below slopes steeper than ~10°. In cases with very small upslope catchments, the MLT beds thin to zero over distances of ~10-20 m from the foot of a slope, while in an area where catchment was large, MLT beds extend hundreds of meters to a kilometer onto adjacent valley floors. (3) MLT beds are ponded within topographic lows such as gulches, where they have bottom contacts that conform with the surface of underlying strata and top contacts that are flat or that drape and pinch out against the sides of gulches over short lateral distances of ~1-3 m. (4) Large clasts (coarse lapilli and blocks) that are hosted within MLT do not show any signs of sag structures into underlying strata (e.g., Fig. 3E), which indicates that the clasts were deposited from the same concentrated flow as the matrix ash rather than ballistically. This contrasts with similar large clasts that are rooted in LXL horizons, which always are accompanied by a sag structure (which may penetrate into underlying MLT beds, such as in Fig. 5). This is consistent with the parent pyroclastic surges being directly related to explosions in the crater.

Sites North and West of the Crater

The relations between three nearby sites—two located on flat topographic highs on either side of a site at the base of a steep slope—are particularly illustrative of the origin of massive lapilli ash/tuff beds (Fig. 12; see also Valentine et al., 2021b). The sites are ~1100-1200 m north of Ubehebe Crater. Site U20-38 (Fig. 6) is on a flat surface. Site U20-45 is only 50 m away and 10 m lower in altitude, at the base of a steep-sided, 80-m-high mesa on the flat top of which is site U21-7 (Fig. 12). The elevated sites have nearly identical stratigraphy composed almost entirely of laminated and cross-laminated ash, with the higher-altitude U21-7 being ~20% thinner than the lower site and with slightly finer overall grain size. Md_a = 1.9 at U21-7, compared to Md_a = 1.5 at the lower-altitude U20-38, based on "trench" samples through the entire sequence at each site. Coarser-grained horizons, such as the bottom layers of coarse-fine couplets, can be correlated between the sites, and the uppermost of these contains the aforementioned flake-shaped, vesicular basalt lapilli. Site U20-45, at the base of the mesa, also contains the same stratigraphy and correlated layers that total to about the same thickness of LXL as at U20-38, but with the addition of interlayered MLT beds (Figs. 12A and 12B). These beds slightly drape onto the base of the slope and pinch out against it over a 1-2 m distance; at nearby outcrops, the slope includes overhanging ledges of sandstone, and the flat-lying MLT beds simply abut the overhangs. MLT beds gradually thin and disappear over distances of ~15-20 m away from the foot of the slope, which indicates that they have the form of low-profile fans. One of the beds has a fine-ash top that is penetrated by coarse ash and fine lapilli from the overlying LXL layers, which is consistent with the MLT having been inflated and soft shortly after deposition.

The above relations indicate a repeated sequence of events, in which discrete pyroclastic surges deposited LXL facies onto the landscape, and this material rapidly remobilized on the steep slopes to form dry granular flows that traveled downslope and were deposited as MLT fans when they encountered flat ground. The "catchment"

above site U20-45 was convex, so that a limited supply of remobilized material could be supplied to a given granular flow path, and they were of very small volume and traveled limited distances onto the flat ground below. The small granular flows deposited at the break in slope and were not erosive there, thus preserving the full LXL stratigraphy. MLT beds were emplaced between pyroclastic surge events.

Similar relations can be observed at other sites on steep topography north-northeast of the crater; one of these indicates that early Ubehebe Crater deposits and part of the underlying S-scoria fall were stripped from slopes of 15° or more uphill from a break in slope (from 15° to 5°). The initial granular flows at this location (U21-8; Table A1) must have been erosive even on the 5° slope, because only patches of S-scoria remain between substrate boulders, and most of the LXL sequence is missing; after the initial erosive phase, granular flows deposited a wedge of MLT just downstream of the break in slope, and two LXL horizons, totaling 20 cm thick, are preserved between these MLT beds. The indication that granular flows stripped and included S-scoria explains why MLT ash has a higher content of basalt relative to lithic grains compared to LXL/thinly bedded lapilli tuff (Fig. 9; note that S-scoria underlies Ubehebe Crater deposits north and east of the crater, but to the west and south the deposits are also underlain by basalt-dominated ejecta from P Crater, which would have the same effect on componentry).

West of Ubehebe Crater, site U20-33 (Fig. 10G) also records interlayering of LXL and MLT horizons. The total thickness of deposits here is 5.1 m, of which laminated and cross-laminated horizons comprise 2.5 m and massive lapilli ash/tuff beds comprise 2.6 m. Several of the eight MLT beds contain single-clast-thick, concentrated zones of matrix-supported basalt lapilli, some of which are continuous across the ~10 m of lateral exposure, while others come and go over distances of decimeters to meters. These impart a crudely stratified appearance to the massive beds (also see Crowe and Fisher, 1973). Some MLT beds grade in their upper few centimeters to thin (1–3 cm), laminated ash horizons that could be interpreted as deposits

of pyroclastic surges sourced at the crater that were emplaced in between concentrated flows; alternatively, they may record small ash-cloud surges associated with the granular flows. Although the general slope at this location is a shallow ~5–7° (northwestward), we infer that the concentrated flows were fed by remobilization of pyroclastic surge deposits on the steeper, 15–20° slopes leading to P Crater above.

Eastern and Southern Gulches

Gulches east and south, and within ~1 km, of Ubehebe Crater's center provide important examples of MLT facies within narrow and steep-sided drainage channels. These gulches, carved into fanglomerate, were present prior to the eruption and have been re-established by erosion as discussed above for East Gulch. Some MLT horizons are flattopped and form wedges against gulch sides, which are typically mantled by 10-20 cm of S-scoria fallout (e.g., Fig. 13A). We infer that these horizons were deposited by granular flows that initiated on the steep slopes of Tin Mountain several hundred meters to the south (Fig. 1) and traveled down as channelized flows in gulch bottoms. Where preserved, MLT that was deposited in the centers or axes of gulches has flat tops, and some beds drape onto adjacent gulch slopes, which suggests that they may have received locally derived contributions from steep gulch slopes (Fig. 13B). Alternatively, the draping geometry could be the result of post-emplacement deflation and compaction (Valentine et al., 2021b). At many gulch sites east of the crater, MLT beds are most abundant in the upper portions of the stratigraphic sequence (Figs. 2-4, 13B, and 13C), which suggests the arrival of concentrated granular flows, initiated some distance upstream, after much of the ballistic and pyroclastic surge deposits were emplaced. This does not necessarily indicate that the concentrated flows began late in the sequence; they may have arrived later at sites down-gulch due to the relatively slow speeds of the flows.

One site ~960 m south-southeast of the crater center is useful for understanding the origin of

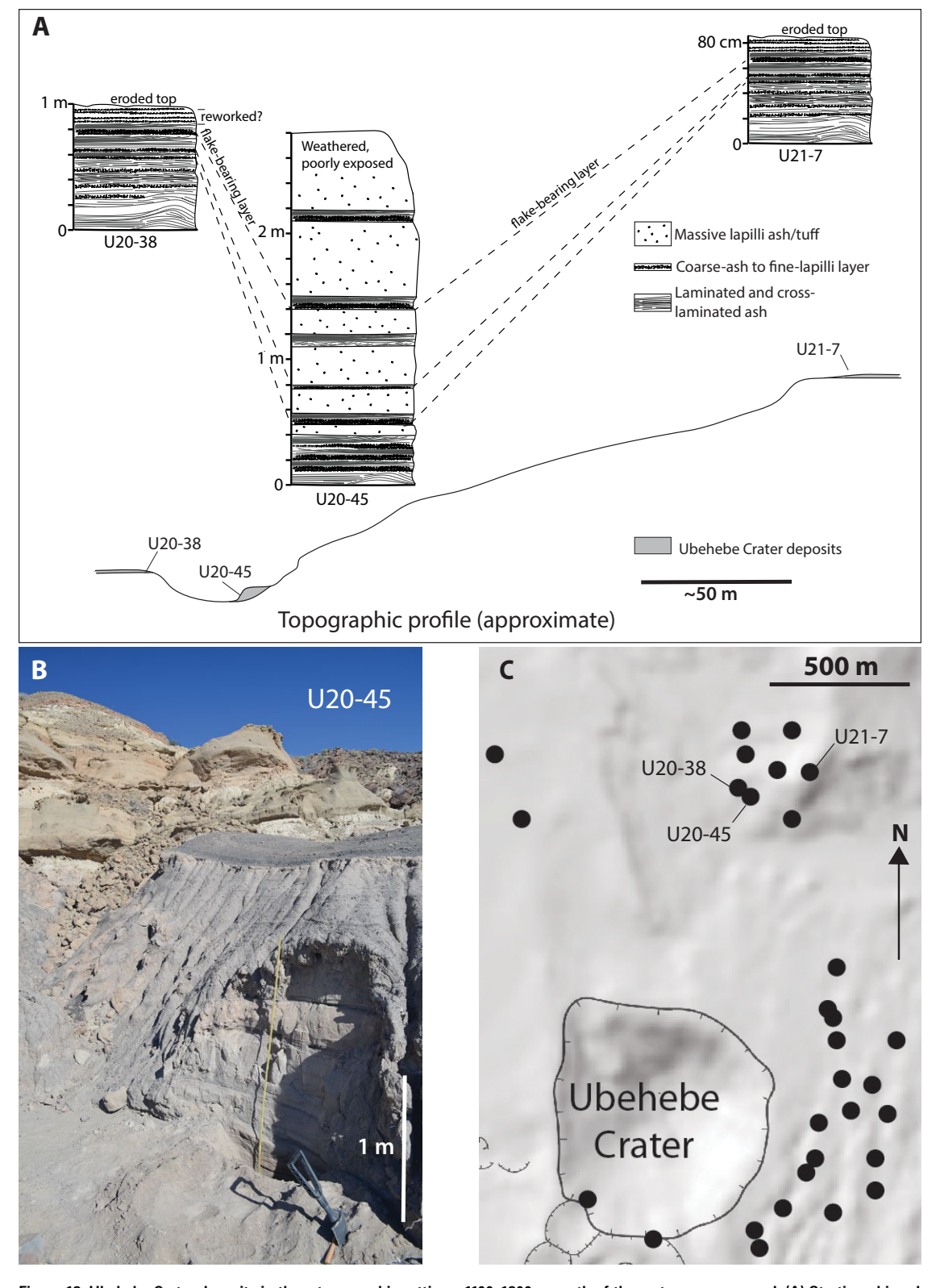
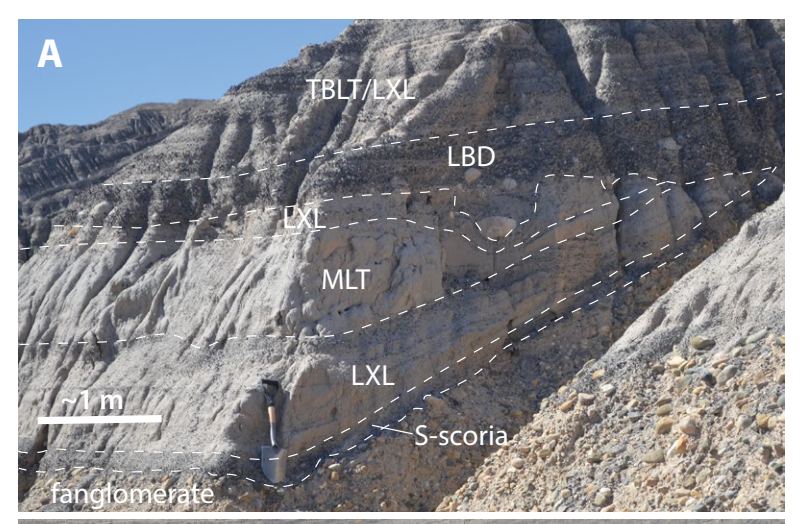


Figure 12. Ubehebe Crater deposits in three topographic settings, 1100–1200 m north of the crater, are compared. (A) Stratigraphic columns for sites U20-38, U20-45, and U21-7, with correlations indicated by dashed lines, and locations with respect to topographic profile (gray indicates Ubehebe deposits). (B) Photograph of U20-45 shows relationship between deposits and pre-eruptive topography at U20-45. (C) Location of sites relative to Ubehebe Crater (from Fig. 1).





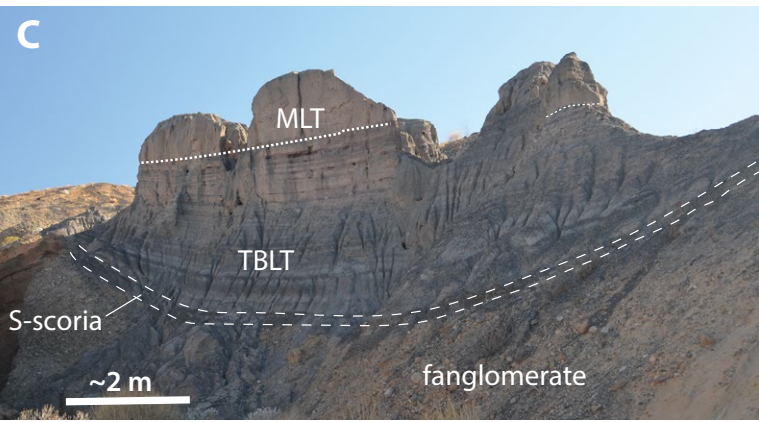


Figure 13. Photographs show massive lapilli ash/tuff (MLT) beds in gulches east of Ubehebe Crater. (A) MLT with minor interstratified laminated and cross-laminated (LXL) ash horizons form a flat-topped wedge against edge of gulch. (B) View northward along a gulch. Dashed lines indicate contact of Ubehebe deposits with older fanglomerate and record the gulch topography prior to eruption. Dotted lines show basal contacts of MLT beds that thin against gulch sides and are thickest and flat-topped in center of gulch as illustrated by two small, butte-like remnants. (C) Remnant of small gulch-filling sequence, with S-scoria fallout mantling fanglomerate, overlain by thinly bedded lapilli tuff (TBLT) with increasing proportions of LXL and thin MLT beds, capped by a flat-lying MLT bed. LBD—lapilli- and block-dominated beds.

4

granular flows that deposited massive lapilli tuff (Fig. 14). This site is in the approximately east-westtrending Gulch 1 of Fierstein and Hildreth (2017), at a location where exposures oriented roughly perpendicular to the channel axis show the lateral transition in facies. Here, an LXL horizon transitions downslope to MLT that thickens toward the channel axis (left in Fig. 14A), with a bottom contact that conforms to the underlying slope of strata and a top contact that becomes subhorizontal. In detail, this transition involves the disruption and progressive mixing of LXL (Figs. 14B and 14C) through soft-sediment deformation processes. Even the thickest part of the MLT bed shown in Figure 14A preserves, upon close inspection, relict laminae that occur in domains a few centimeters in size that are jumbled but incompletely homogenized. Although inaccessible for detailed observation, the opposite side of the channel shows additional examples of soft-sediment deformation of some LXL horizons. This deformation is mainly in the form of small thrust faults, which produce a flame-like appearance with repetition of fine layers interbedded with coarser ones (Fig. 14D; see also Douillet et al., 2015). This is interpreted to record the initial slumping and remobilization of LXL (and, to a lesser extent, thinly bedded lapilli tuff) horizons, which in this outcrop were arrested before completion of the process of mixing that produced homogeneous MLT beds. Like MLT beds observed here and elsewhere, these disrupted horizons are sandwiched between undeformed LXL/thinly bedded lapilli tuff horizons,

which indicates that the initiation of deposit remobilization in these cases occurred between pyroclastic surge events. We think that many MLT beds were emplaced by granular flows that were initiated by these slumping and mixing processes, but it is also possible that some granular flows were initiated immediately upon the accumulation of pyroclastic surge deposits onto the steepest slopes, potentially bypassing the processes documented above. Note that many of the MLT beds at Ubehebe contain vague shear structures with slight variations in grain size and composition, which may be relicts of original stratification.

Farther south is a series of west-northwesttrending drainages that originate just below the ridgeline of Tin Mountain. In this area, the steep (10–15°) upper slopes of Tin Mountain are devoid of Ubehebe deposits, but they are present in downstream reaches of channels where gradients are low. About 1500 m south-southwest of the crater center, sites U21-17 and U21-28 record the transition in deposits from the foot of a steep hill into distinct emplacement units that can be correlated ~200 m downstream (Figs. 15A and 15B). At all of the documented sites in this drainage, the basal 6-7 cm comprises gray to tan, laminated ash that is inferred to record the initial passage of pyroclastic surges over the sites (the top is indicated by line 1 between Figs. 15F and 15G). This horizon is overlain by 8 cm of fine-grained, massive ash with scattered coarse ash that is capped by a distinctive, 1-2-cm-thick layer of coarse ash to fine lapilli (mostly basalt, but with scattered lithic clasts) where coarser individual grains penetrate up to 2 cm into the massive ash bed (line 2, Figs. 15F and 15G). These are interpreted to record deposition from a thin, granular flow that formed by remobilization of the initial surge deposits from steep slopes upstream, which was followed by either a brief period of fine lapilli fallout while the massive bed was still inflated and soft or by initial deposition from a pyroclastic surge (i.e., the beginnings of a coarse layer from a coarse-fine couplet, which was overprinted by subsequent granular flow before completion of the couplet). Two MLT layers, both sampled along the flow path (Figs. 15C-15G), totaling 46-52 cm thickness, overlie the lower sequence;

the upper of these two contains more abundant fine-medium basalt lapilli (matrix supported), especially in its middle ~10 cm, and the beds are separated locally by a 1-cm-thick very fine-ash layer or by a cryptic, irregular to gradational (over ~2 cm) contact that indicates local erosion/mixing by a granular flow into underlying soft MLT (contact is indicated by line 3 in Figs. 15F and 15G). A horizon of LXL that is up to 14 cm thick, but is also locally truncated or missing, overlies the lower MLT beds, and the lower portion of the LXL horizon exhibits flame-like structures that indicate downslope shearing (top and bottom of horizon is indicated by lines 4 and 5 between Figs. 15F and 15G). Finally, an upper MLT bed is capped by a 2-3 cm LXL horizon (between lines 6 and 7 in Figs. 15F and 15G) that is truncated by an erosional surface and overlain by fluvially reworked deposits. This upper MLT bed ranges from 8 cm at the upstream site (U21-17b) to ~1 m just 20 m downstream (U21-17c), where there is a confluence with a tributary drainage. Its central portion is rich in lapilli, giving it an appearance of a lapilli "stringer" on weathered surfaces, and it contains scattered metamorphic cobbles that are inferred to be derived from loose surface rubble on the steep slopes above. Grain size and componentry are essentially constant within the sampled MLT beds along their preserved flow lengths (Figs. 15C and 15D), although the LXL horizons between MLT beds locally are absent, which indicates erosion by granular flows. Overall, this series of sites demonstrates common themes of MLT beds interlayered with LXL horizons that record deposition of MLT between surge events (perhaps interrupting surge deposition in one case). LXL horizons sum to ~20 cm thickness, which may approximate the total thickness derived directly from pyroclastic surges at this distance, although it is uncertain how much additional LXL material was removed by concentrated flows.

An additional 500 m to the south, at a distance of ~2000 m from crater center, lies another drainage that has a larger upstream catchment than most, in the form of tributary channels that drain a concave-west portion of the Tin Mountain ridgeline (Fig. 16A). Just downstream of the confluence of most of these tributaries, the drainage is focused

into an ~5-m-wide bedrock channel with a sudden drop of ~5 m, which we refer to as the Notch waterfall. A major tributary, which also drains a substantial catchment, converges with the main channel just downstream of the waterfall. Stream gradients are typically 10° or more above the Notch waterfall and only ~3° below it, as the main channel eventually spreads onto an alluvial fan. Massive lapilli ash/tuff beds are the dominant facies of Ubehebe Crater deposits in this drainage, with very little variation in grain-size characteristics and componentry in the 1-mm fraction, but they range from as little as 50 cm thick in the upstream exposures to more than 6 m just below the Notch waterfall (Figs. 16B-16D). At most locations in the drainage, MLT lacks clearly defined internal contacts and overlies 8-10 cm of laminated and cross-laminated ash recording initial pyroclastic surges that reached the area (these are deposited atop basaltic, lapilli-rich material linked with P Crater). MLT is preserved as remnants of flat-topped, ponded deposits that abut adjacent channel sides (Figs. 17A and 17B). Crude stratification is related to matrix-supported zones of concentrated basalt lapilli, which in many cases appear in a deposit near or just downstream of channel confluences. The appearance of these concentration zones is enhanced on weathered surfaces (Fig. 17C). Middle and upper portions of ponded MLT deposits, especially near confluences, contain scattered metamorphic and sedimentary cobbles that in places are concentrated into matrix-supported lenses up to ~1 m thick (Fig. 17D). Elongate cobbles are commonly imbricated (clasts dip upstream) and, where well-developed, the cobble-rich lenses are also imbricated with respect to adjacent lenses. The cobbles were derived from loose fanglomerate rubble on the steep slopes of Tin Mountain.

The character of MLT deposits in this drainage is consistent with our interpretation wherein they were derived from remobilized, fresh pyroclastic surge deposits on Tin Mountain slopes; the remobilization and motion of the resulting granular flows were capable of stripping and entraining earlier Ubehebe deposits, eventually including loose pre-eruptive material on the paleosurfaces. The concentrated granular flows carried material

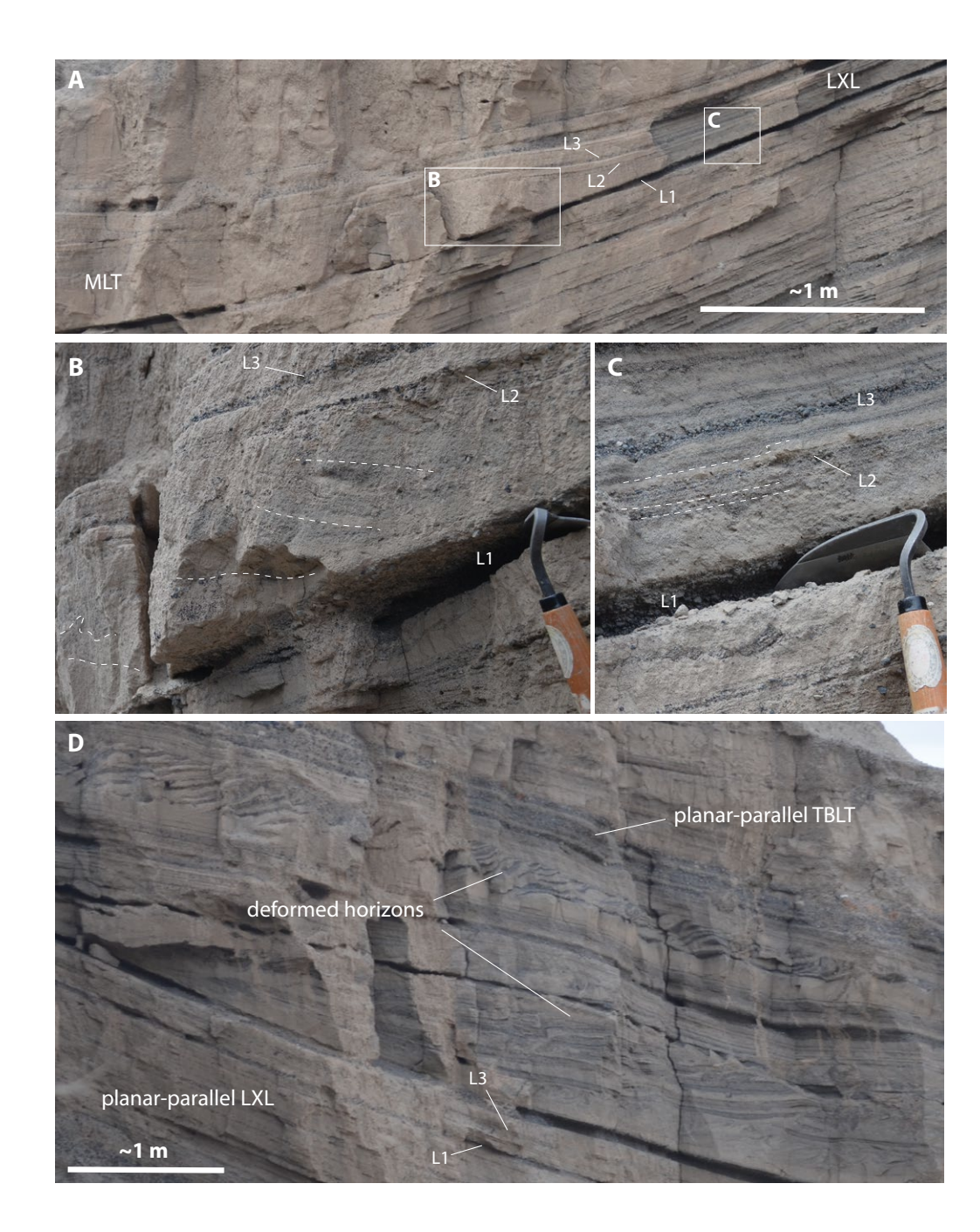


Figure 14. Photographs demonstrate the role of soft-sediment deformation in the formation of massive lapilli ash/tuff (MLT) beds; outcrop is approximately perpendicular to channel axis, with sloping beds parallel to paleochannel side (site U21-1, Table A1). (A) View of leftward (downslope) thickening of a horizon in otherwise planar parallel-laminated and cross-laminated (LXL) ash with interbedded, thinly-bedded lapilli tuff (TBLT) horizons. Locations of areas detailed in panels B and C are outlined. Note that the left-thickening deposit of interest is sandwiched between planar parallel-bedded horizons. For reference, L1, L2, and L3 refer to lapilli layers in other parts of the figure. (B) Detail of texture of horizon just at it begins to thicken and take on a massive appearance. Close observation reveals domains of disrupted laminae (some are highlighted with dashed lines). (C) Only ~1 m upslope, laminae are planar parallel. Tool handle is ~2 cm wide. (D) Exposure in opposite side of channel illustrates deformed horizons (mainly due to small-scale, slump-related faulting) sandwiched between undisturbed, planar parallel horizons. The soft-sediment deformation records early phases of the formation of massive ash/tuff (MLT) beds by disruption and mixing of mainly LXL horizons and associated thickening that occured during pauses between pyroclastic surges.

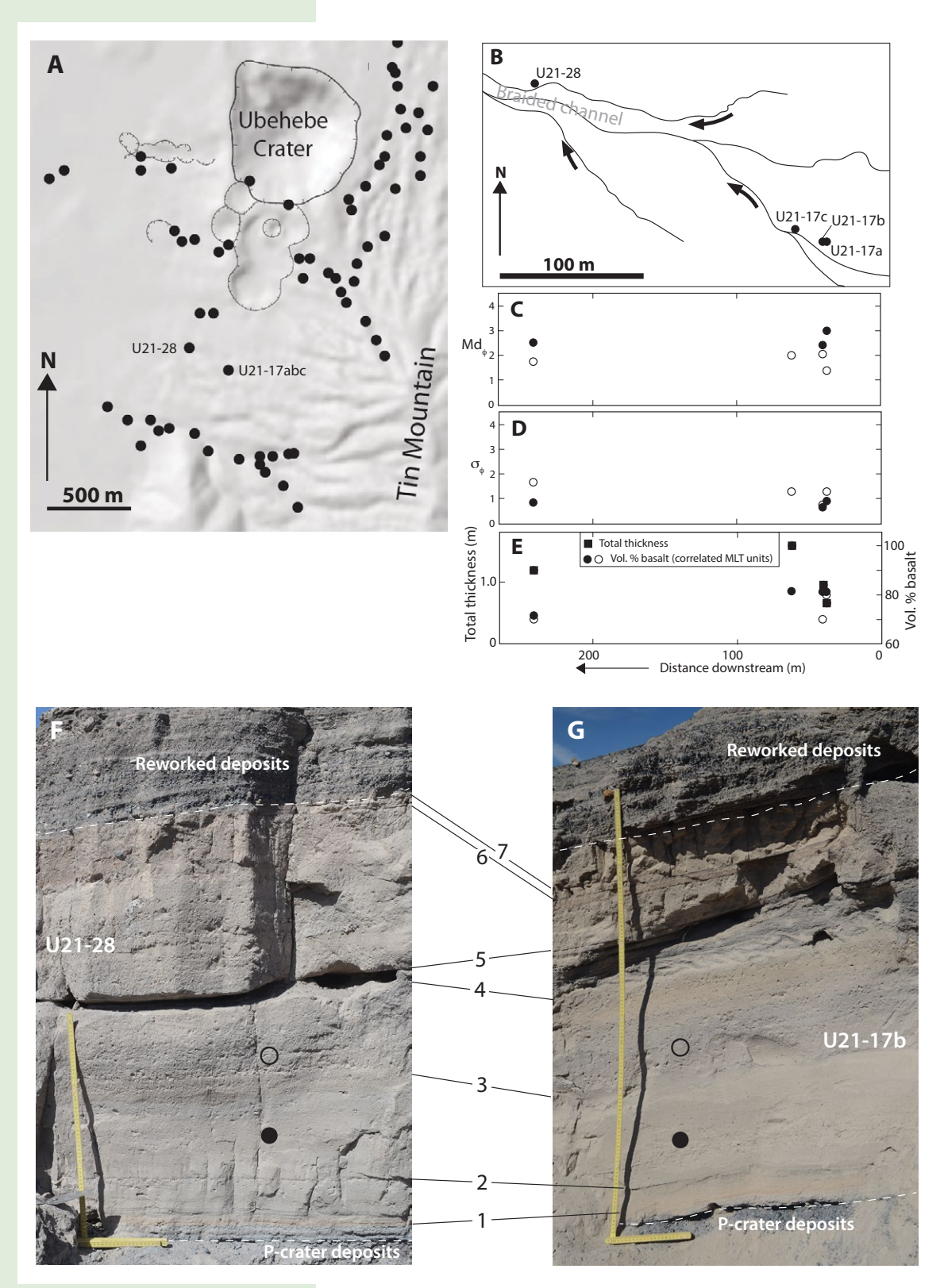


Figure 15. Massive lapilli ash/ tuff (MLT) beds along channels/ flow paths are mapped and grain-size characteristics are plotted at a sequence of locations ~1.5 km south of Ubehebe Crater's center. (A) Locations of stations (black dots) with respect to Ubehebe Crater (from Fig. 1). (B) Simplified map of drainage: thin lines are channels, and arrows indicate transport directions (downstream). Labeled dots are study sites. The western ~150 m is a 30-m-wide braided channel. (C) Median ted against distance. Closed and open circles in panels C-G correspond to two MLT beds that can be correlated downstream. (D) Inman sorting (σ_{ϕ}) against distance. Grain-size parameters are relatively constant over ~200 m distance. (E) Total thickness (closed squares) and basalt-clast content in 1 mm fraction (circles) at selected sites. Deposits are thinnest at site U21-17a, where they were emplaced against a steep slope, and thickest ~25 m downstream (site U21-17c), near a confluence with adjacent drainage, and then thin gradually downstream. (F and G) Photographs of Ubehebe deposits (underlain by P-Crater deposits and truncated on top by reworked deposits) at sites U21-28 and U21-17b. Connecting lines show correlated contacts between internal strata. Open and closed circles correspond to locations of samples plotted with open and closed symbols in panels C-E. Vertical part of ruler in panel F is 60 cm, and in panel G it is 120 cm.

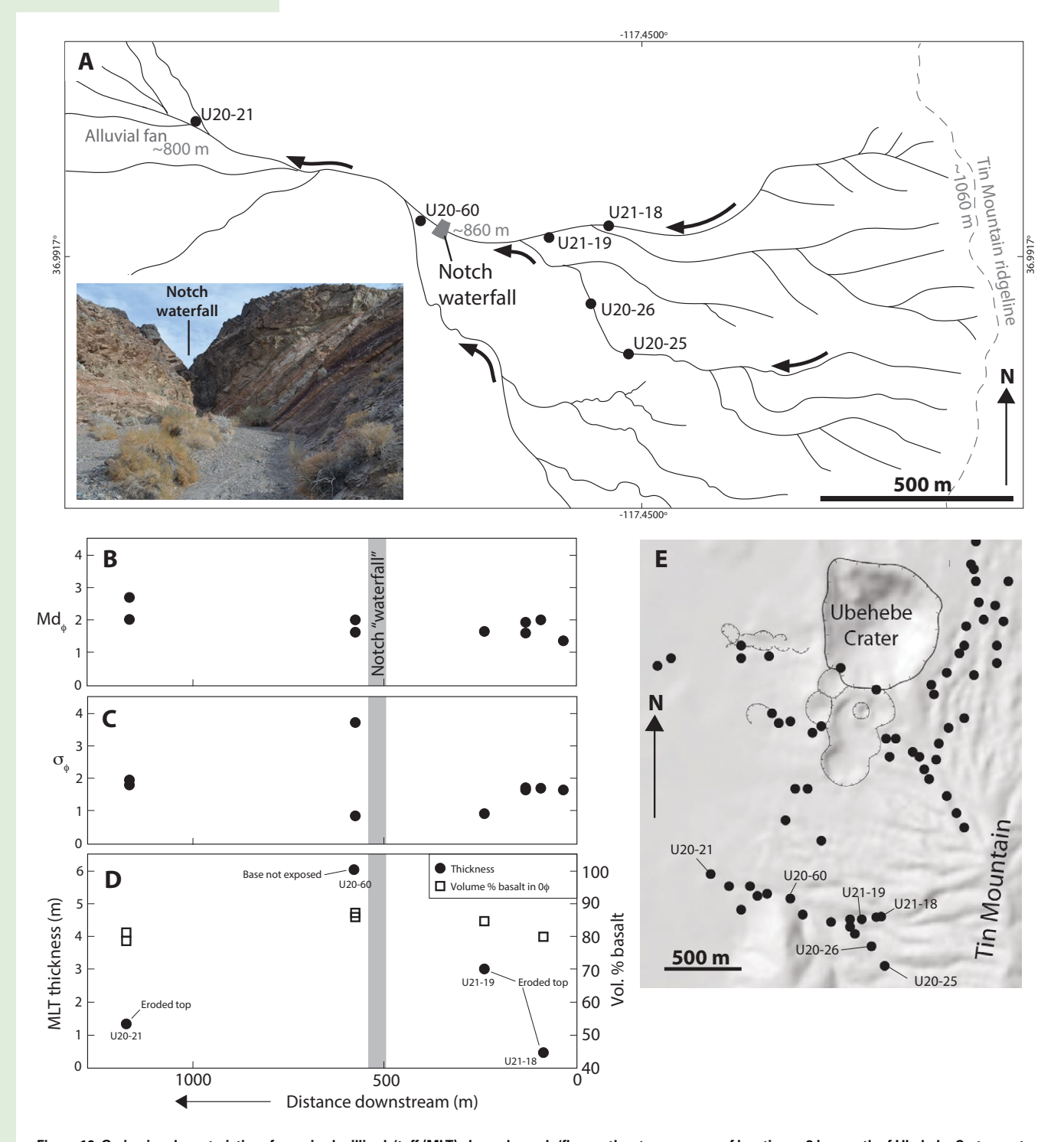


Figure 16. Grain-size characteristics of massive lapilli ash/tuff (MLT) along channels/flow paths at a sequence of locations ~2 km south of Ubehebe Crater center are shown. (A) Simplified map of drainage: thin lines are channels, and arrows indicate transport direction (downstream). Indicated are site locations (black dots), the ridgeline of Tin Mountain to the east (dashed line), an alluvial fan to the west that is supplied by the drainage, and the Notch waterfall, where most of the upstream channels converge and must pass through an ~5-m-wide channel and a vertical drop of ~5 m (see inset photo taken from just downstream). Altitudes of these features are indicated in gray. (B) Median diameter in ϕ units (Md $_{\phi}$) are plotted against distance. (C) Inman sorting (σ_{ϕ}) is plotted against distance. Grainform a lapilli-rich zone in the lower ~1.5 m of the deposit. (D) Thickness (closed circles) and basalt-clast content in 1 mm fraction (open squares) at selected sites. Upstream, most sites where MLT beds begin to occur are typically 1 m or less thick. Thicknesses increase downstream, especially near confluences. The thickest observed MLT is just below the Notch waterfall. Near the head of the alluvial fan, massive deposits have thinned substantially, and multiple emplacement units are visible, some of which have erosive, U-shaped channel contacts with underlying MLT beds. (E) Location of stations with respect to Ubehebe Crater (from Fig. 1).

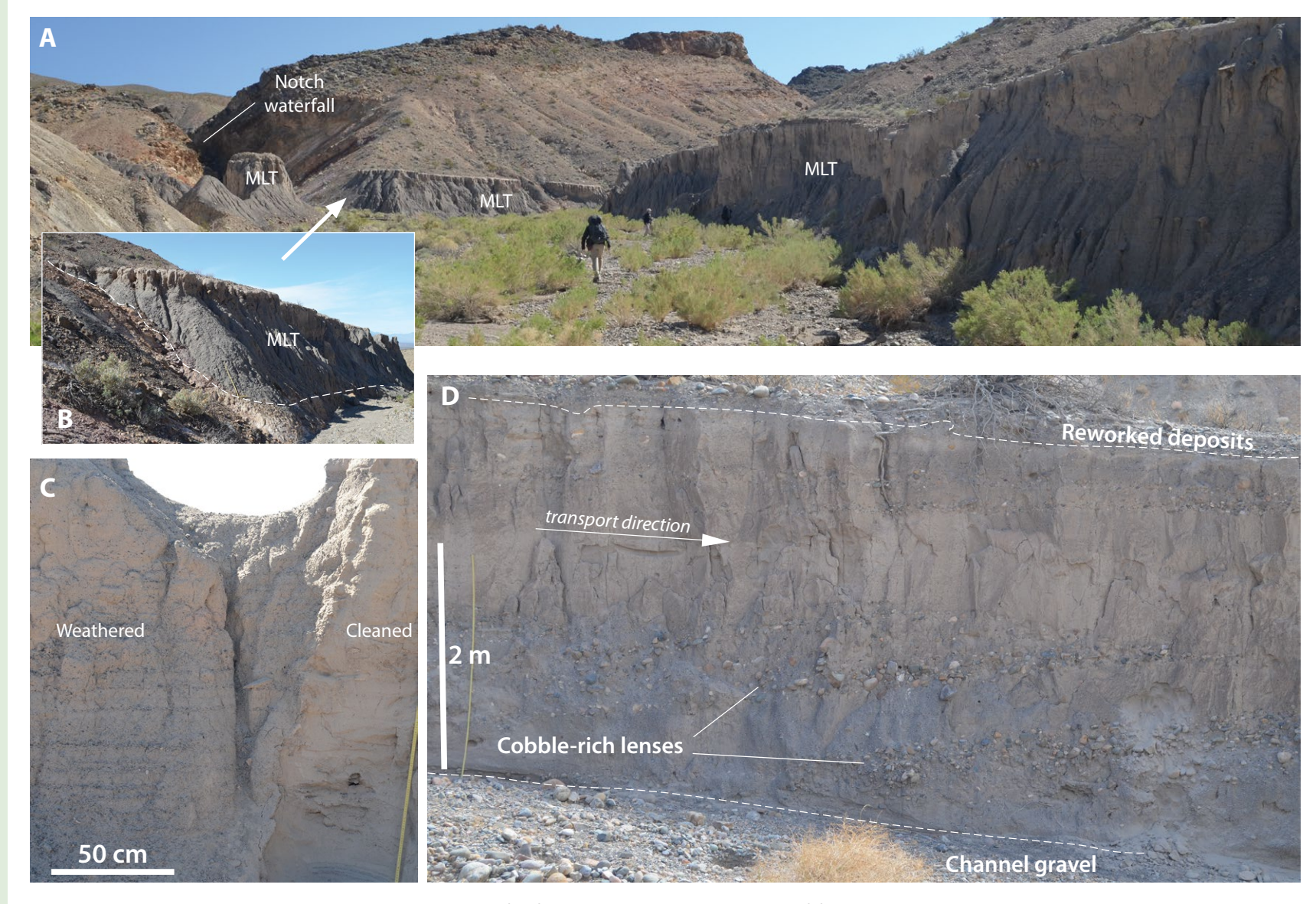


Figure 17. Photographs show massive lapilli ash/tuff (MLT) deposits in the Notch waterfall drainage. (A) Remnants of thickly ponded MLT deposits, locally exceeding 6 m thick, just below the Notch waterfall. (B) Detail shows contact of MLT with channel sides and flat upper surface. Note that in both panels A and B, the lighter-colored top of the deposit is sunbleached and weathered, rather than a different layer. (C) Exposure ~420 m downstream of Notch waterfall illustrates basalt lapilli concentrations on weathered surface, which impart crude stratification to the deposit. (D) Cobble-rich lenses, imbricated with respect to each other, in ponded deposits upstream of the Notch waterfall.

at least 800 m downstream of the Notch waterfall onto an alluvial fan (site U20-21; Figs. 16A and 16E); here, two MLT emplacement units are easily distinguished, separated by an ~10-cm-thick horizon of planar parallel-laminated ash. This LXL horizon is locally disrupted by upward folding and flame like structures. Because the slope is quite shallow here (2-3°), it is unlikely that this deformation is related to slumping; instead, it records shearing by granular flow that deposited the overlying MLT bed. The presence of a vaguely defined U-shaped channel (~2 m wide and 30 cm deep) filled by MLT and cut into underlying MLT combines with the soft-sediment structures to indicate that some of the granular flows had erosive capacity here. We suggest that, farther upstream, any interbedded LXL deposits were completely removed by more energetic granular flows, and individual MLT emplacement units mixed with underlying units such that clear contacts are not preserved; however, the lapilli concentration zones likely record cryptic emplacement units or pulsing of granular flows that were sourced from different parts of the upstream tributary system and arrived in rapid succession. As the granular flows spread onto the alluvial fan and decelerated, they became less erosive such that contacts and some LXL horizons are preserved. Similar, but thinner, domains of MLT formed on the eastern side of Tin Mountain and extend up to ~1 km onto the adjacent valley floor there.

Although the terrain south of the Notch waterfall drainage is composed of steep mountains, in small and isolated valleys, and their alluvial fans to the south, as far as 7130 m from crater center, similar 0.45-1.1-m-thick beds of MLT are preserved. This demonstrates that Ubehebe Crater-sourced pyroclastic surges traveled at least that far in that direction, and although they are no longer preserved on the steep mountainsides, they did remobilize to form granular flows that are locally preserved as ponded, massive lapilli tuff. We note that in one of these distal drainages and in the two discussed above, there is a sharp, erosional contact with overlying fluvially reworked deposits and local debris flow deposits. In most cases, the latter are more strongly indurated than underlying MLT beds, which is probably a result of their wet

emplacement as opposed to the MLT-producing dry granular flows.

DISCUSSION

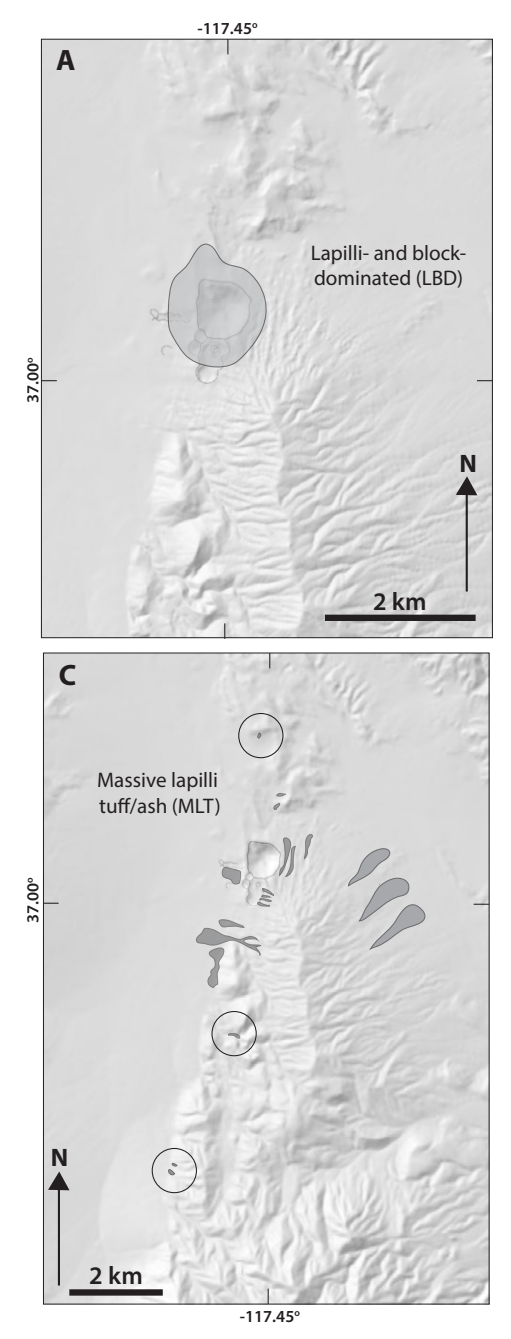
The Ubehebe Crater deposits resulted from three main pyroclastic emplacement processes, each of which is recorded by the main facies types. Lapilli- and block-dominated beds were deposited by ballistic curtains and/or by clast showers from collimated jets. They extend several hundred meters from the crater center (Fig. 18A), except immediately north of the crater, where they extend ~1 km, transitioning with distance from continuous beds to lenticular clusters of lapilli and blocks. The farther northern limit extends from a topographic low on the crater rim, which might have facilitated ballistic curtains in that direction via inclined jets (Valentine et al., 2015; Graettinger et al., 2015b). Individual coarse lapilli and blocks were also deposited ballistically by explosions throughout the sequence.

Thinly bedded lapilli tuffs and laminated and cross-laminated ash horizons were deposited by pyroclastic surges. Thinly bedded lapilli tuff is found mainly within several hundred meters of crater center, although as with lapilli- and block-dominated beds, thinly bedded lapilli tuff beds are found ~1 km immediately north of the crater, radially from the low point on the crater rim. This may be a result of northward-inclined explosion jets or due to reflection of outgoing pyroclastic currents off the high part of the rim and subsequent flow over the lower northern rim (e.g., White and Schmincke, 1999; Valentine et al., 2015; Graettinger et al., 2015b; Sweeney et al., 2018). Pyroclastic surges extended at least 9 km from the crater center to the north and 7 km to the south (Fig. 18B). While the overall transport of particles by pyroclastic surges was outward from the crater, dune-form migration data indicate that local bed-load transport was down the axes of pre-existing gulches and channels (also see Crowe and Fisher, 1973). Lower portions of individual pyroclastic surges with denser, higher particle-concentration were blocked and directed downslope, regardless of the overall

transport direction, a process that was also documented in the 1980 lateral blast deposit at Mount St. Helens, Washington (Fisher, 1990). Our data do not support the systematic decrease in dune-form wavelength with radial distance that was reported by Wohletz and Sheridan (1979), and within a small distance, or even within a single exposure, dune forms can have different sizes and migration directions. This is likely a result of the LXL facies having been deposited by many individual surges, each with different transport and deposition properties. The topographic blocking process also complicates this, since at any given location in a channel, pulses of pyroclastic surge may have arrived at different times due to flow down different upstream tributaries, even if the surge was generated by a single discrete explosion at the vent.

Also similar to the Mount St. Helens blast deposit, Ubehebe pyroclastic surge runout may have been reduced to the east of the crater due to nearly orthogonal ridges and gulches, which enhanced sedimentation and reduced the particle content as a function of distance (Doronzo et al., 2010), but it may have been maximized where topographic trends were subparallel to the overall transport direction (Fisher, 1990; note that this is somewhat uncertain because of potential burial of the deposits by subsequent alluvial action east of the crater). To the north, the topographic trend is defined by a series of mesas and cuestas that rise ~50-100 m above the valley floor. South of the crater, the main topographic trend is the ~1100 m a.s.l. ridgeline of Tin Mountain (Fig. 1), which rises ~300 m above surrounding valley floors and apparently deflected pyroclastic surges such that they stayed entirely or at least mostly to the west and east of the ridge crest. Ballistic curtains and pyroclastic surges were produced by many separate explosions at the crater. Only the most energetic extended to the distal areas indicated in Figures 18A and 18B.

MLT beds were emplaced primarily by concentrated granular flows that originated from dry remobilization of pyroclastic surge deposits off steep slopes (Fig. 18C). Remobilization occurred through slumping, soft-sediment deformation, and homogenization of fresh, still-inflated LXL deposits,



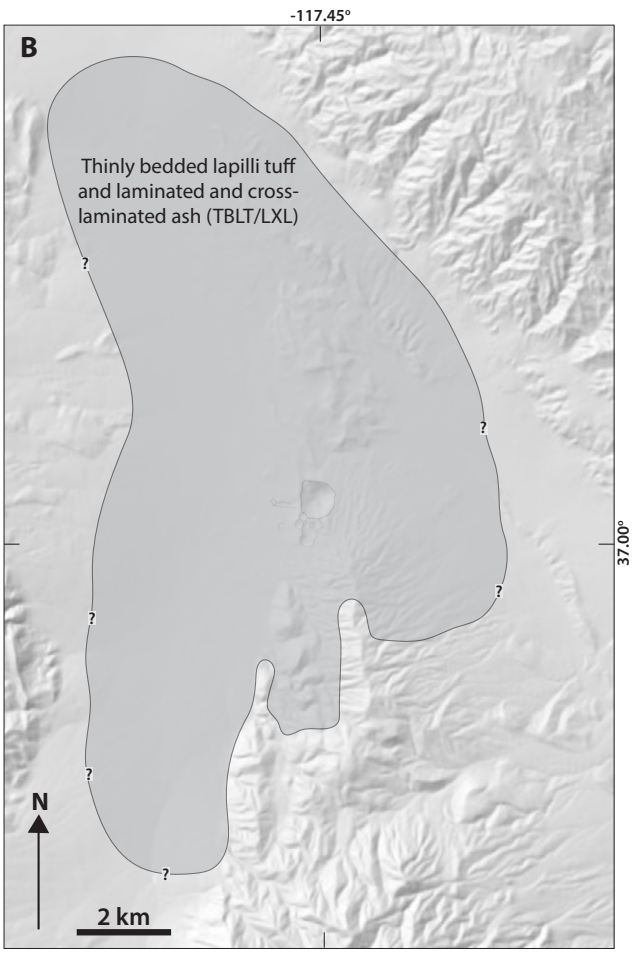


Figure 18. Documented distributions of the three facies of Ubehebe Crater deposits are shown (Note that panel A has a different scale than panels B and C). (A) Lapilli- and block-dominated deposits (LBD), which are interpreted to have been emplaced by ballistic processes, are found within several hundred meters of the crater center and extend slightly farther (to ~1 km) just north of the crater. (B) Extent of thinly bedded lapilli tuff (TBLT) and laminated and cross-laminated (LXL) deposits, which are inferred to record pyroclastic surges. Question marks indicate areas where limits are difficult to define due to burial beneath alluvial sediments. (C) Massive lapilli ash/tuff facies (MLT), which are interpreted to record granular flows of rapidly remobilized pyroclastic surge deposits off steep slopes (circled areas enclose small patches of MLT in distal areas). Note that there are multiple deposits of each of these facies, which for LBD and TBLT/LXL record numerous individual explosions of different energies.

likely within minutes or tens of minutes of initial deposition, while pore-gas pressure remained high, although this is poorly constrained (Valentine et al., 2021b). Additionally, rapid sedimentation from suspended load and immediate drainage (termed by Fisher, 1990, as "almost deposited" material; also see Druitt et al., 2002) may have fed granular flows, but evidence of this would not be preserved. Mobility of the granular flows was facilitated by high gas-pore pressures inherited from the fresh surge deposits and retained due to the abundant fine-medium ash in the flows, and potentially by differential motion between particles and gas during flow and as deposits aggraded at the bases of the flows (Roche, 2012). High pore pressures and "fluffiness" of both fresh LXL and MLT deposits is evidenced by abundant examples of tiny impact sags caused by deposition of coarse ash to fine lapilli on the tops of just-deposited beds, as if grains fell onto inflated powder (see also Valentine et al., 2021b). In some places, granular flows were completely depositional, rather than erosive, and the complete pyroclastic surge sequence is preserved with MLT beds emplaced between surges. In other places with larger upstream catchments for remobilized surge deposits, or where slopes were greater than ~5°, the granular flows were alternately erosive and depositional, such that parts of the primary surge sequence, or of MLT beds emplaced earlier, are missing. Concentrated granular flows moved independently down drainages, extending several hundred meters to ~1 km onto adjacent valley floors, which provides a complicating factor to consider for hazards at maar volcanoes near steep terrain. Similar considerations were made by Druitt et al. (2002) for surge-derived pyroclastic flows at Soufrière Hills, Montserrat, where the parent currents were ash-cloud surges associated with primary block-and-ash flows.

Both Crowe and Fisher (1973) and Wohletz and Sheridan (1979) attributed massive beds to direct deposition from pyroclastic surge clouds. Crowe and Fisher (1973) attributed the massive beds to high particle concentration in the lower parts of surges that were focused or funneled down channels; White and Schmincke (1999) also came to this conclusion about very similar massive beds

associated with phreatomagmatic activity on the island of La Palma, Canary Islands. While it is possible that some MLT beds originated that way, most that we observed at Ubehebe are more easily explained as granular flows sourced from rapidly remobilized surge deposits or "almost deposits." Wohletz and Sheridan (1979) inferred that the massive beds represent a transitional condition of outgoing pyroclastic surges that deposit primarily "sandwave" facies proximally and planar parallelbedded facies distally (although they only traced the deposits at Ubehebe a maximum of ~10% of their runout distance, mostly along East Gulch). While our evidence indicates that this is not the case, we agree that finer-grained distal deposits tend to be planar parallel-laminated (Fig. 6), while cross-stratified deposits and dune forms are more common within ~2 km of crater center. These lateral changes are similar to those described by Vazguez and Ort (2006) at Haskie tuff ring in Arizona. Finally, Leat and Thompson (1988) described Miocene phreatomagmatic centers in Colorado that have very similar sequences of stratified and cross-stratified deposits, which they attributed to pyroclastic surges, slump or soft-sediment deformation structures, and massive channel-filling deposits. They inferred that the deposits were emplaced wet due to the latter two features, even though they did not find additional evidence such as accretionary lapilli or deposits plastered against steep surfaces. Leat and Thompson (1988) discussed a range of mechanisms that could have formed the massive beds, ranging from slumping of wet surge deposits to collapse of wet eruption columns and "effusion" of clast-water slurries from the vents. These interpretations involving liquid water as a key factor contrast with our interpretation of formation of concentrated granular flows in a dry state during activity at Ubehebe Crater (Valentine et al., 2021b).

CONCLUSIONS

We described and interpreted deposits associated with the final, Ubehebe Crater-forming, phreatomagmatic explosive phase of the complex, monogenetic Ubehebe volcanic center. The work builds upon seminal studies of cross-stratified deposits and dune forms and their relations to pyroclastic surges (Fisher and Waters, 1970; Crowe and Fisher, 1973). In addition to pyroclastic surges, pyroclasts were transported and deposited by ballistic curtains and as individual ballistic clasts proximally, and by dry, concentrated granular flows formed by rapid remobilization of fresh surge deposits off steep slopes. Runout of pyroclastic surges appears longest where they are parallel to the trends of topographic highs. The lower, denser portions of pyroclastic surges were blocked by steep topography and traveled down channels while the overriding cloud moved radially from source. Surge deposits on steep slopes rapidly remobilized via slumping and mixing to form dry, concentrated granular flows that traveled independently of the pyroclastic surges and therefore are a complicating factor for hazard assessments. Although similar surge-derived, concentrated flows have been described elsewhere (Fisher, 1990; Druitt et al., 2002), to our knowledge Ubehebe may be the first case where such processes have been identified at a maar volcano. Work is underway to apply time-dependent, three-dimensional, multiphase fluid dynamics modeling to the Ubehebe deposits with the goal of quantitatively linking deposit characteristics with explosion and flow conditions.

ACKNOWLEDGMENTS

We thank Meredith Cole, Patrick Bobbitt, and Xander Percy for work on granulometry and componentry and, along with Anastasia Rashchupkina and Brandon Keim, assistance in the field. Jessica Ball, Lucia Gurioli, Michael Ort, and associate editor Christopher Spence provided careful reviews that sharpened the manuscript. The work was supported by the U.S. Geological Survey's Volcano Hazards Program and by National Science Foundation grant EAR-2035260 to G.A. Valentine and was conducted with permission from Death Valley National Park. Any use of trade, firm, or product names is for descriptive purposes only and does not imply endorsement by the U.S. government.

APPENDIX

Table A1 provides location information for all sites that were documented in detail, as well as summary information on the deposit characteristics at each site.

TABLE A1. LOCATIONS AND CHARACTERISTICS OF STUDY SITES

Site	Latitude (°N)	Longitude (°W)	Distance (direction) from crater center (m)	Total thickness* (m)	Setting	Facies present [†]	Samples collected	
J19-4/ J21-3	37.0127	117.4442	650 (NE)	3.2	Flat-lying deposits enter ~100-m-wide channel, near East Gulch mouth.	MLT, LXL, LBD	7	Reworked material on top.
U19-5	37.0124	117.4441	630 (NE)	2.5	Center of ~50-m-wide channel.	LXL, MLT, LBD	0	
J19-6	37.0103	117.4426	620 (E)	3.5	Confluence of two drainages.	LXL, LBD, MLT	6	Eroded top.
J19-8	37.0075	117.4450	570 (E)		Steep side of East Gulch.	LBD, LXL, MLT	0	Basal contact dips of ~40°.
J19-9/ J21-4	37.0064	117.4459	580 (E)	16.5	Flat-lying deposits near center of ~80-m-wide paleochannel.	LBD, LXL, MLT	9	Eroded top.
J19-14	37.0106	117.4436	630 (SE)	4.8	Flat-lying deposits near center of ~70-m-wide paleochannel.	LXL, LBD, MLT	0	Eroded top, local cut-and-fill with reworked deposits.
J19-17	37.0007	117.4473	1090 (SSE)	2.2	Flat-lying deposits at confluence of channels.	LXL, MLT, LBD	0	Eroded top.
J19-24	37.0063	117.4440	730 (ESE)	7.2	Flat-lying deposits near confluence of channels.	LBD, LXL, MLT	5	Eroded top with reworked deposits.
J20-3	37.0145	117.4392	1130 (E)	0.05	Low bank within ~100-m-wide channel.	Indeterminant	0	Bioturbated with eroded top.
J20-4	37.0140	117.4391	1120 (E)	0.22	Remnant of ponded deposit within ~10-m-wide channel.	MLT,LXL	2	Eroded top.
J20-7	37.0109	117.4378	1140 (E)	2.05	Low terrace within ~15-m-wide channel.	MLT, LXL	4	Eroded top.
J20-8	37.0109	117.4351	1400 (E)	0.15	Low terrace at bend in channel.	LXL	1	Eroded top.
J20-9	37.0090	117.4357	1340 (E)	8.0	Low terrace within ~50-m-wide channel.	MLT, LXL	0	Eroded top.
J20-13/ J21-16	37.0127	117.4347	1450 (NE)	1.05	Low terrace on alluvial fan.	MLT, LXL	1	Eroded top.
J20-20	36.9920	117.4543	2030 (S)	2.5	Below confluences, ~100 m upstream from Notch waterfall.	MLT, LXL	0	Eroded top.
J20-21	36.9949	117.4629	2000 (SSW)	1.18	Alluvial fan ~700 m downstream from Notch waterfall.	MLT, LXL	2	Eroded top.
J20-22	36.9940	117.4616	2030 (SSW)	2.2	Alluvial fan ~560 m downstream from Notch waterfall.	MLT, LXL	0	Eroded top.
J20-25	36.9895	117.4504	2270 (S)	0.65	Hillside slope, ~530 upstream of Notch waterfall.	MLT, LXL	1	Eroded top.
U20-26	36.9907	117.4514	2140 (S)	1.4	Flat surface in channel bottom, base of steep hill, ~400 m upstream of Notch waterfall.	MLT, LXL	2	Eroded top.
J20-27	36.9932	117.4526	2080 (S)	3.5	Edge of ~20-m-wide channel below confluence of three drainages, ~250 m upstream of Notch waterfall.	MLT	0	Eroded top, littered with alluvial cobbles.
J20-32	37.0072	117.4609	960 (W)	N/A	West-facing slope.	LXL	0	Dune form in upper part of deposits. Not excavated to base.
J20-33	37.0071	117.4588	790 (WSW)	5.4	Below break in slope leading up to P Crater ~50 m S of W-crater rim.	LXL,MLT	7	Eroded top.
J20-34	37.0078	117.4607	950 (WSW)	1.2	Near edge of Y crater.	LXL, MLT	4	Eroded top.
J20-36	37.0027	117.4499	825 (S)	6.0	~45-m-wide channel, lower part of Gulch 1.	MLT, LXL	3	Top locally eroded, locally capped by reworked material.
J20-37	37.0015	117.4503	955 (S)	3.9	~30-m-wide channel, midway along Gulch 2.	MLT, LXL	3	Capped by reworked material.
J20-38	37.0198	117.4478	1120 (N)	0.98	Top of gently sloping (toward crater) mesa.	LXL	4	Eroded top.
J20-39	37.0126	117.4728	1990 (W)	0.37	Flat valley floor.	LXL	3	Eroded top.
J20-40	37.0187	117.4723	2155 (NW)	0.36	Flat valley floor.	LXL	3	Capped by reworked material.
J20-41	37.0206	117.4715	2200 (NW)	0.35	Flat valley floor.	LXL	0	Eroded top, littered with alluvial cobbles.

(continued)

TABLE A1. LOCATIONS AND CHARACTERISTICS OF STUDY SITES (continued)

Site	Latitude (°N)	Longitude (°W)	Distance (direction) from crater center (m)	Total thickness* (m)	Setting	Facies present [†]	Samples collected	
U20-45	37.0194	117.4474	1060 (N)	2.8	Foot of steep mesa side.	MLT, LXL	5	Eroded top, covered with loose scoria lapilli.
U20-47	37.0262	117.4486	1810 (N)	0.2	Mesa-side slope (faces crater).	LXL	2	Eroded top, covered with loose scoria lapilli, some bioturbation.
U20-48	37.0251	117.4514	1670 (N)	0.47	Gently sloping valley floor.	LXL	2	Erosional contact with overlying reworked deposit, some bioturbation.
U20-49	37.0306	117.4511	2280 (N)	0.09	Gently sloping valley floor.	LXL	1	Eroded top, covered by loose scoria lapilli. Upper centimeters are vesicular (A _v).
U20-51	37.0322	117.4510	2670 (N)	0.11	Mesa-side slope (faces crater).	LXL	1	Capped by 2 cm of reworked deposit with poorly developed desert pavement.
U20-52	37.0330	117.4529	2555 (N)	0.51	Drainage channel on vent-facing mesa side.	MLT, LXL	1	Capped by 4 cm of reworked deposit.
U20-53	37.0342	117.4555	2710 (N)	0.15	Mesa side.	MLT, LXL		Eroded top.
U20-55	37.0359	117.4605	3000 (NNW)	0.10	Flat valley floor.	LXL, MLT	3	Capped by 4 cm of reworked deposit.
U20-56	37.0338	117.4602	2770 (NNW)	0.12	Flat valley floor.	LXL, MLT	0	Capped by 3 cm of reworked deposit.
U20-57	37.0310	117.4593	2460 (NNW)	0.16	Flat valley floor.	LXL, MLT	0	
U20-58	36.9939		1985 (SSW)	1.75	~100-m-wide channel at head of alluvial fan ~550 m downstream from Notch waterfall.	MLT, LXL	0	Eroded top.
U20-59	36.9936	117.4589	1960 (SSW)	>3.8	50-m-wide channel, ~310 m downstream from Notch waterfall.	MLT, ?	0	Base not exposed. Eroded top, locally capped by alluvial conglomerate.
U20-60/ U21-21	36.9925	117.4564	2010 (SSW)	>6	60-m-wide channel, ~60 m downstream from Notch waterfall.	MLT, ?	2	Base not exposed. Flat, slightly eroded top.
U20-61	36.9927	117.4607	2220 (SW)	1.5	Small pyroclastic fan at foot of "No-Name Mountain."	MLT, LXL	0	Flat, slightly eroded top.
U20-62	36.9745	117.4603	4040 (SSW)	1.2	~50-m-wide, gently sloping channel below confluences with at least three steep mountainside channels.	MLT	2	Capped by likely debris-flow (lahar) deposit, 0.8 m thick.
U20-63	37.0072	117.4659	1390 (W)	0.58	Flat valley bottom.	LXL	3	Eroded top.
U20-64	37.0068	117.4670	1480 (W)	0.46	Flat valley bottom.	LXL	2	Capped by reworked material.
U21-1	37.0017	117.4480	960 (SSE)	-	Exposure perpendicular to axis of Gulch 1.	LXL, TBLT	0	Transition from laminated to massive deposits.
U21-7	37.0203	117.4451	1235 (NNE)	0.6	Mesa top above U20-45 (~80 m higher).	LXL	3	Eroded top.
U21-8	37.0215	117.4461	1340 (N)	1.05	W-sloping channel (~10 m wide) on mesa side.	MLT, LXL	1	Eroded top.
U21-9	37.0213	117.4477	1300 (N)	0.6	Gently ventward-sloping surface.	LXL	1	Eroded top.
U21-10	37.0118	117.4415	830 (ENE)	0.42	Flat gravel terrace surface in ~50-m-wide channel draining Tin Mountain.	LXL, MLT	1	Eroded top.
U21-13	37.0070	117.4423	820 (ESE)	~3	Near axis of ~20-m-wide channel draining Tin Mountain.	MLT, LXL, LBD	3	Upper 2 m not accessible.
U21-17	see U20-17	see U20-17	1545 (S)	0.67–1.7	~20-m-wide channel draining Tin Mountain.	MLT, LXL	8	Deposits thicken away from foot of hill. Eroded top.
U21-18	36.9924	117.4510	1965 (S)	0.55	Confluence of two channels into a single one, ~30 m wide.	MLT, LXL	1	Eroded top.
U21-19	36.9921	117.4526	2000 (S)	~3	~15-m-wide channel, 145 m downstream from site U21-18.	MLT	1	Eroded top, locally capped by fluvial deposits. Massive deposits with cobble lenses.
U21-20	36.9917	117.4528	2020 (S)	~3	~20-m-wide channel.	MLT, LXL		Eroded top, locally capped by fluvial deposits. Massive deposits with cobble lenses.

(continued)

TABLE A1. LOCATIONS AND CHARACTERISTICS OF STUDY SITES (continued)

Site	Latitude (°N)	Longitude (°W)	Distance (direction) from crater center (m)	Total thickness* (m)	Setting	Facies present [†]	Samples	
U21-22	37.0037	117.4577	950 (SW)	1.35	Near break in slopes from P Crater.	LXL, MLT, LBD	3	Eroded top.
U21-23	37.0032	117.4553	, ,	1.7	Steep upper slopes just below P Crater.	LXL, LBD	2	Eroded top.
U21-24	37.0187	117.4563	1075 (NNW)	>1.2	Ventward-facing upper slopes of low ridge.	LXL, LBD	2	Base not exposed. Eroded top.
U21-25	37.0207	117.4574	1325 (NNW)	>1	Ventward-facing slope of low ridge.	LXL	1	Only basal ~0.5 m exposed, upper portion likely correlates to exposure in site U21-24.
U21-26	37.0259	117.4638	2115 (NW)	0.36	Flat valley floor.	LXL	2	Weathered top, no apparent erosion.
U21-27	37.0233	117.4627	1810 (NW)	0.48	Flat valley floor.	LXL		Weathered top, upper few centimeters A_{ν} , no apparent erosion.
U21-28	36.9978	117.4575	1500 (SW)	1.2	~40-m-wide channel just above head of alluvial fan, 270 m downstream from site U21-17.	MLT, LXL	3	Eroded top, overlain by fluvial deposits.
U22-3	37.0815	117.4942	8960 (NNW)	0.05	~2-m-high side of channel cut into pre- Ubehebe playa deposits.	LXL	1	Isolated distal remnant of Ubehebe Crater deposits, overlain by fluvial deposits.
U22-4	37.0736	117.4812	7700 (NNW)	0.05	Side of channel cut into pre-Ubehebe playa deposits.	LXL	0	Isolated distal remnant of Ubehebe Crater deposits, overlain by fluvial deposits.
U22-5	37.0131	117.4396	1030 (ENE)	0.2	Near base of ~5-m-deep channel side, which faces away from crater.	LXL	0	Upper several centimeters weathered.
U22-6	37.0009	117.4294	1870 (E)	1.2	Alluvial fan fed by channel that heads on steep NE slopes of Tin Mountain.	MLT	0	MLT contains cobble concentration zones. Ubehebe Crater deposits overlain by loose cobbles.
U22-7	37.0293	117.4932	4280 (NW)	~0.03	Alluvial fan sourced from mountains west of Ubehebe.	LXL	0	Deposit disrupted by bioturbation.
U22-8	37.0290	117.4896	4060 (NW)	~0.11	Alluvial fan sourced from mountains west of Ubehebe.	LXL	0	Upper 4 cm of weathered ash.
U22-11	36.9984	117.4731	7130 (SSW)	0.45	Upper fan near mouth of small canyon.	MLT	0	Ubehebe Crater deposit underlain and overlain by loose angular cobbles.
U22-12	36.9496	117.4723	7000 (SSW)	0.45	Upper fan near mouth of small canyon.	MLT	0	Ubehebe Crater deposit underlain and overlain by loose angular cobbles.
U22-14	36.9857	117.4704	3230 (SW)	0.16	Flat valley floor.	LXL	0	Upper several centimeters weathered.
U22-16	37.0103	117.4179	2880 (E)	0.41	Bank of channel on edge of alluvia fan fed from Tin Mountain.	MLT	0	Erosive upper contact with overlying fluvial sand and gravel.
U22-18	37.0020	117.4229	2630 (ESE)	1.3	Alluvial fan fed from Tin Mountain.	MLT	0	Eroded/weathered top littered with cobbles.
U22-19	36.9970	117.8485	2760 (SE)	~1	Alluvial fan fed from Tin Mountain.	MLT	0	Eroded/weathered top littered with cobbles.
U22-20	37.0034	117.4173	3060 (ESE)	~1	Alluvial fan fed from Tin Mountain.	MLT	0	Eroded/weathered top littered with cobbles.
UB-6-1	37.0454	117.4209	4770 (NE)	0.01	Alluvial fan fed from mountains to NE of Ubehebe Crater.	LXL	0	Orange—tan very fine to fine ash; well-defined layer in sharp contact with alluvial fan deposit above and intact S-fall below.
Sec-59	37.0570	117.4310	5540 (NNE)	0.01	Channel draining mountains to NE of Ubehebe Crater.	LXL	0	Orange—tan very fine ash in sharp contact with fluvial deposits above and intact S-fall below.
Sec-60	37.0869	117.4823	8960 (NNW)	0.001- 0.003	Alluvial fan fed from mountains to NE of Ubehebe Crater.	LXL	0	Pale orange very fine ash overlain by fluvial deposits; rests on intact S-fall.
Sec-63	37.0777	117.4727	7770 (N)	0.01	Channel draining mountains to NE of Ubehebe Crater.	LXL	0	Pale orange very fine ash overlain by aeolian sand; in sharp contact with S-fall below.

Note: *Total thickness of undisturbed deposits from Ubehebe Crater only, not including potential underlying deposits from preceding phases of activity or reworked deposits that may overlie undisturbed material. Only reported for sites where total thickness was directly measured.

†LBD—lapilli- and block-dominated lapilli tuff; LXL—laminated and cross-laminated; MLT—massive lapilli tuff. Listed in order of decreasing proportion of total thickness.

REFERENCES CITED

- Allen, J.R.L., 1970a, A quantitative model of climbing ripples and their cross-laminated deposits: Sedimentology, v. 14, p. 5–26, https://doi.org/10.1111/j.1365-3091.1970.tb00179.x.
- Allen, J.R.L., 1970b, Physical Processes of Sedimentation: London, George Allen & Unwin, 248 p.
- Belousov, A., Voight, B., and Belousova, M., 2007, Directed blasts and blast-generated pyroclastic density currents: A comparison of the Bezymianny 1956, Mount St. Helens 1980, and Soufrière Hills, Montserrat 1997 eruptions and deposits: Bulletin of Volcanology, v. 69, p. 701–740, https://doi.org/10.1007/s00445-006-0109-v.
- Breard, E.C.P., Lube, G., Cronin, S.J., Fitzgerald, R., Kennedy, B., Scheu, B., Montanaro, C., White, J.D.L., Tost, M., Procter, J.N., and Moebis, A., 2014, Using the spatial distribution and lithology of ballistic blocks to interpret eruption sequence and dynamics: August 6 2022 Upper Te Maari eruption, New Zealand: Journal of Volcanology and Geothermal Research, v. 286, p. 373–386, https://doi.org/10.1016/j.jvolgeores.2014.03.006.
- Breard, E.C.P., Lube, G., Cronin, S.J., and Valentine, G.A., 2015, Transport and deposition processes of the hydrothermal blast of the 6 August 2012 Te Maari eruption: Mt. Tongariro: Bulletin of Volcanology, v. 77, 100, https://doi.org/10.1007 /s00445-015-0980-5.
- Brosch, E., and Lube, G., 2020, Spatiotemporal sediment transport and depositional processes in experimental dilute pyroclastic density currents: Journal of Volcanology and Geothermal Research, v. 401, https://doi.org/10.1016/j.jvolgeores.2020.106946.
- Champion, D.E., Cyr, A., Fierstein, J., and Hildreth, W., 2018, Monogenetic origin of Ubehebe Crater maar volcano, Death Valley, California: Paleomagnetic and stratigraphic evidence: Journal of Volcanology and Geothermal Research, v. 354, p. 67–73, https://doi.org/10.1016/j.jvolgeores.2017.12.018.
- Crowe, B.M., and Fisher, R.V., 1973, Sedimentary structures in base-surge deposits with special reference to cross-bedding, Ubehebe Craters, Death Valley, California: Geological Society of America Bulletin, v. 84, p. 663-682, https://doi.org/10.1130/0016-7606(1973)84-663:SSIBDW>2.0.C0:2.
- Dellino, P., Zimanowski, B., Büttner, R., La Volpe, L., Mele, D., and Sulpizio, R., 2007, Large-scale experiments on the mechanics of pyroclastic flows: Design, engineering, and first results: Journal of Geophysical Research: Solid Earth, v. 112, B04202, https://doi.org/10.1029/2006JB004313.
- Dellino, P., Dioguardi, F., Doronzo, D.M., and Mele, D., 2019, The rate of sedimentation from turbulent suspension: An experimental model with application to pyroclastic density currents and discussion on grain-size dependence of flow runout: Sedimentology, v. 66, p. 129–145, https://doi.org /10.1111/sed.12485.
- Dellino, P., Dioguardi, F., Doronzo, D.M., and Mele, D., 2020, A discriminatory diagram of massive versus stratified deposits based on sedimentation and bedload transport rates. Experimental investigation and application to pyroclastic density currents: Sedimentology, v. 67, p. 2013–2039, https:// doi.org/10.1111/sed.12693.

- Dioguardi, F., and Dellino, P., 2014, PYFLOW: A computer code for calculation of the impact parameters of Dilute Pyroclastic Density Currents (DPDC) based on field data: Computers & Geosciences, v. 66, p. 200–210, https://doi.org/10.1016/j.cageo.2014.01.013.
- Doronzo, D.M., Valentine, G.A., Dellino, P., and de Tullio, M.D., 2010, Numerical analysis of the effect of topography on deposition from dilute pyroclastic density currents: Earth and Planetary Science Letters, v. 300, p. 164–173, https://doi.org/10.1016/j.epsl.2010.10.003.
- Douillet, G.A., 2021, The supercritical question for pyroclastic dune bedforms: An overview: Sedimentology, v. 68, p. 1698– 1727, https://doi.org/10.1111/sed.12859.
- Douillet, G.A., Pacheco, D.A., Kueppers, U., Letort, J., Tsang-Hin-Sun, E., Bustillos, J., Hall, M., Ramón, P., and Dingwell, D.B., 2013, Dune bedforms produced by dilute pyroclastic density currents from the August 2006 eruption of Tungurahua volcano, Ecuador: Bulletin of Volcanology, v. 75, https:// doi.org/10.1007/s00445-013-0762-x.
- Douillet, G.A., Taisne, B., Tsang-Hin-Sun, È., Müller, S.K., Kueppers, U., and Dingwell, D.B., 2015, Syn-eruptive, softsediment deformation of deposits from dilute pyroclastic density current: Triggers from granular shear, dynamic pore pressure, ballistic impacts and shock waves: Solid Earth, v. 6, p. 553–572, https://doi.org/10.5194/se-6-553-2015.
- Druitt, T.H., Calder, E.S., Cole, P.D., Hoblitt, R.P., Loughlin, S.C., Norton, G.E., Ritchie, L.J., Sparks, R.S.J., and Voight, B., 2002, Small-volume, highly mobile pyroclastic flows formed by rapid sedimentation from pyroclastic surges at Soufrière Hills Volcano, Montserrat: An important volcanic hazard, in Druitt, T.H., and Kokelaar, B.P., eds., The Eruption of Soufrière Hills Volcano, Montserrat, from 1995–1999: Geological Society, London, Memoir 21, p. 263–279, https://doi.org/10.1144/GSL.MEM.2002.021.01.12.
- Fierstein, J., and Hildreth, W., 2017, Eruptive history of the Ubehebe Crater cluster, Death Valley, California: Journal of Volcanology and Geothermal Research, v. 335, p. 128–146, https://doi.org/10.1016/j.jvolgeores.2017.02.010.
- Fisher, R.V., 1990, Transport and deposition of a pyroclastic surge across an area of high relief: The 18 May 1980 eruption of Mount St. Helens, Washington: Geological Society of America Bulletin, v. 102, p. 1038–1054, https://doi.org/10.1130/0016-7606(1990)102<1038:TADOAP>2.3.CO;2.
- Fisher, R.V., and Schmincke, H.-U., 1984, Pyroclastic Rocks: Heidelberg, Springer-Verlag, 471 p., https://doi.org/10.1007/978 -3-642-74864-6.
- Fisher, R.V., and Waters, A.C., 1970, Base surge bed forms in maar volcanoes: American Journal of Science, v. 268, p. 157–180, https://doi.org/10.2475/ajs.268.2.157.
- Fisher, R.V., Heiken, G., and Hulen, J.B., 1997, Volcanoes: Crucibles of Change: Princeton, New Jersey, Princeton University Press, 317 p., https://doi.org/10.1515/9780691238210.
- Graettinger, A.H., and Valentine, G.A., 2017, Evidence for the relative depths and energies of phreatomagmatic explosions recorded in tephra rings: Bulletin of Volcanology, v. 79, 88, https://doi.org/10.1007/s00445-017-1177-x.
- Graettinger, A.H., Valentine, G.A., Sonder, I., Ross, P.-S., White, J.D.L., and Taddeucci, J., 2014, Maar-diatreme geometry and deposits: Subsurface blast experiments with variable explosion depth: Geochemistry, Geophysics, Geosystems, v. 15, p. 740–764, https://doi.org/10.1002/2013GC005198.

- Graettinger, A.H., Valentine, G.A., Sonder, I., Ross, P.-S., and White, J.D.L., 2015a, Facies distribution of ejecta in analog tephra rings from experiments with single and multiple subsurface explosions: Bulletin of Volcanology, v. 77, 66, https://doi.org/10.1007/s00445-015-0951-x.
- Graettinger, A.H., Valentine, G.A., and Sonder, I., 2015b, Circum-crater variability of deposits from discrete, laterally and vertically migrating volcanic explosions: Experimental evidence and field implications: Journal of Volcanology and Geothermal Research, v. 308, p. 61–69, https://doi.org/10.1016/j.jvolgeores.2015.10.019.
- Gurioli, L., Harris, A.J., Colò, L., Bernard, J., Favalli, M., Ripepe, M., and Andronico, D., 2013, Classification, landing distribution, and associated flight parameters for a bomb field emplaced during a single major explosion at Stromboli, Italy: Geology, v. 41. p. 559–562. https://doi.org/10.1130/G33967.1.
- Leat, P.T., and Thompson, R.N., 1988, Miocene hydrovolcanism in NW Colorado, USA, fueled by explosive mixing of basic magma and wet unconsolidated sediment: Bulletin of Volcanology, v. 50, p. 229–243, https://doi.org/10.1007/BF01047486.
- Lefebvre, N.S., White, J.D.L., and Kjarsgaard, B.A., 2013, Unbedded diatreme deposits reveal maar-diatreme-forming eruptive processes: Standing Rocks West, Hopi Buttes, Navajo Nation, USA: Bulletin of Volcanology, v. 75, 739, https://doi.org/10.1007/s00445-013-0739-9.
- Middleton, G.V., and Southard, J.B., 1978, Mechanics of Sediment Movement: Society of Economic Paleontologists and Mineralogists Short Course 3, 259 p.
- Moore, J.G., 1967, Base surge in recent volcanic eruptions: Bulletin Volcanologique, v. 30, p. 337–363.
- Roche, O., 2012, Depositional processes and gas pore pressure in pyroclastic flows: An experimental approach: Bulletin of Volcanology, v. 74, p. 1807–1820, https://doi.org/10.1007 /s00445-012-0639-4.
- Roche, O., 2015, Nature and velocity of pyroclastic density currents inferred from models of entrainment of substrate lithic clasts: Earth and Planetary Science Letters, v. 418, p. 115–125, https://doi.org/10.1016/j.epsl.2015.03.001.
- Roche, O., Niño, Y., Manganey, A., Brand, B., Pollock, N., and Valentine, G.A., 2013, Dynamic pore-pressure variations induce substrate erosion by pyroclastic flows: Geology, v. 41, p. 1107–1110, https://doi.org/10.1130/G34668.1.
- Roche, O., Buesch, D.C., and Valentine, G.A., 2016, Slow-moving and far-travelled dense pyroclastic flows during the Peach Spring super-eruption: Nature Communications, v. 7, https:// doi.org/10.1038/ncomms10890.
- Self, S., Kienle, J., and Huot, J.-P., 1980, Ukinrek Maars, Alaska, II. Deposits and formation of the 1977 craters: Journal of Volcanology and Geothermal Research, v. 7, p. 39–65, https:// doi.org/10.1016/0377-0273(80)90019-0.
- Sparks, R.S.J., Bursik, M.I., Carey, S.N., Gilbert, J.S., Glaze, L.S., Sigurdsson, H., and Woods, A.W., 1997, Volcanic Plumes: Chichester, UK, John Wiley & Sons, Ltd., 574 p.
- Sweeney, M.R., Grosso, Z.S., and Valentine, G.A., 2018, Topographic controls on a phreatomagmatic maar-diatreme eruption: Field and numerical results from the Holocene Dotsero volcano (Colorado, USA): Bulletin of Volcanology, v. 80, 78, https://doi.org/10.1007/s00445-018-1253-x.
- Taddeucci, J., Valentine, G.A., Sonder, I., White, J.D.L., Ross, P.-S., and Scarlato, P., 2013, The effect of pre-existing craters on the initial development of explosive volcanic eruptions: An

- experimental investigation: Geophysical Research Letters, v. 40, p. 507–510, https://doi.org/10.1002/grl.50176.
- Valentine, G.A., 1987, Stratified flow in pyroclastic surges: Bulletin of Volcanology, v. 49, p. 616–630, https://doi.org/10.1007
- Valentine, G.A., 2012, Shallow plumbing systems for small-volume basaltic volcanoes, 2: Evidence from crustal xenoliths at scoria cones and maars: Journal of Volcanology and Geothermal Research, v. 223–224, p. 47–63, https://doi.org/10 .1016/j.jvolgeores.2012.01.012.
- Valentine, G.A., 2020, Initiation of dilute and concentrated pyroclastic currents from collapsing mixtures and origin of their proximal deposits: Bulletin of Volcanology, v. 82, 20, https:// doi.org/10.1007/s00445-020-1366-x.
- Valentine, G.A., and Connor, C.B., 2015, Basaltic volcanic fields, in Sigurdsson, H., Houghton, B., McNutt, S.R., Rymer, H., and Stix, J., eds., The Encyclopedia of Volcanoes (2nd edition): Amsterdam, Elsevier, p. 423–439, https://doi.org/10 .1016/B978-0-12-385938-9.00023-7.
- Valentine, G.A., and White, J.D.L., 2012, Revised conceptual model for maar-diatreme: Subsurface processes, energetics, and eruptive products: Geology, v. 40, p. 1111–1114, https:// doi.org/10.1130/G33411.1.
- Valentine, G.A., Shufelt, N.L., and Hintz, A.R.L., 2011, Models of maar volcanoes, Lunar Crater (Nevada, USA): Bulletin of Volcanology, v. 73, p. 753–765, https://doi.org/10.1007 /s00445-011-0451-6.

- Valentine, G.A., White, J.D.L., Ross, P.-S., Amin, J., Taddeucci, J., Sonder, I., and Johnson, P.J., 2012, Experimental craters formed by single and multiple buried explosions and implications for volcanic craters with emphasis on maars: Geophysical Research Letters, v. 39, https://doi.org/10.1029 /2012GL053716.
- Valentine, G.A., Graettinger, A.H., and Sonder, I., 2014, Explosion depths for phreatomagmatic eruptions: Geophysical Research Letters, v. 41, p. 3045–3051, https://doi.org/10.1002/2014GI.060096.
- Valentine, G.A., Graettinger, A.H., Macorps, É., Ross, P.-S., White, J.D.L., Döhring, E., and Sonder, I., 2015, Experiments with vertically and laterally migrating subsurface explosions with applications to the geology of phreatomagmatic and hydrothermal explosion craters and diatremes: Bulletin of Volcanology, v. 77, 15, https://doi.org/10.1007/s00445-015-0901-7
- Valentine, G.A., White, J.D.L., Ross, P.-S., Graettinger, A.H., and Sonder, I., 2017, Updates to concepts on phreatomagmatic maar-diatremes and their pyroclastic deposits: Frontiers in Volcanology, v. 5, https://doi.org/10.3389/feart.2017.00068.
- Valentine, G.A., Ort, M.H., and Cortés, J.A., 2021a, Quaternary basaltic volcanic fields of the American Southwest: Geosphere, v. 17, p. 2144–2171, https://doi.org/10.1130 /GES02405.1.
- Valentine, G.A., Fierstein, J., and White, J.D.L., 2021b, Soft sediment deformation in dry pyroclastic deposits at Ubehebe

- Crater, Death Valley, California: Geology, v. 49, p. 211–215, https://doi.org/10.1130/G48147.1.
- Vazquez, J.A., and Ort, M.H., 2006, Facies variation of eruption units produced by the passage of single pyroclastic surge currents, Hopi Buttes volcanic field, USA: Journal of Volcanology and Geothermal Research, v. 154, p. 222–236, https:// doi.org/10.1016/j.jvolgeores.2006.01.003.
- Weit, A., Roche, O., Dubois, T., and Manga, M., 2018, Experimental measurement of the solid particle concentration in geophysical turbulent gas-particle mixtures: Journal of Geophysical Research: Solid Earth, v. 123, p. 3747–3761, https://doi.org/10.1029/2018JB015530.
- White, J.D.L., and Houghton, B.F., 2006, Primary volcaniclastic rocks: Geology, v. 34, p. 677–680, https://doi.org/10.1130/G22346.1.
- White, J.D.L., and Schmincke, H.-U., 1999, Phreatomagmatic eruptive and depositional processes during the 1949 eruption on La Palma (Canary Islands): Journal of Volcanology and Geothermal Research, v. 94, p. 283–304, https://doi.org /10.1016/S0377-0273(99)00108-0.
- White, J.D.L., and Valentine, G.A., 2016, Magmatic versus phreatomagmatic fragmentation: Absence of evidence is not evidence of absence: Geosphere, v. 12, p. 1478–1488, https:// doi.org/10.1130/GES01337.1.
- Wohletz, K.H., and Sheridan, M.F., 1979, A model of pyroclastic surge, in Chapin, C.E., and Elston, W.E., eds., Ash-Flow Tuffs: Geological Society of America Special Paper 180, p. 177–194, https://doi.org/10.1130/SPE180-p177.